LETTER

doi:10.1038/nature22306

Surrogate Wnt agonists that phenocopy canonical Wnt and β-catenin signalling

Claudia Y. Janda[1]*, Luke T. Dang[2]*, Changjiang You[3], Junlei Chang[4], Wim de Lau[5], Zhendong A. Zhong[6], Kelley S. Yan[4], Owen Marecic[7], Dirk Siepe[1], Xingnan Li[4], James D. Moody[2], Bart O. Williams[6], Hans Clevers[5], Jacob Piehler[3], David Baker[2], Calvin J. Kuo[4] & K. Christopher Garcia[1]

Wnt proteins modulate cell proliferation and differentiation and the self-renewal of stem cells by inducing β-catenin-dependent signalling through the Wnt receptor frizzled (FZD) and the co-receptors LRP5 and LRP6 to regulate cell fate decisions and the growth and repair of several tissues[1]. The 19 mammalian Wnt proteins are cross-reactive with the 10 FZD receptors, and this has complicated the attribution of distinct biological functions to specific FZD and Wnt subtype interactions. Furthermore, Wnt proteins are modified post-translationally by palmitoylation, which is essential for their secretion, function and interaction with FZD receptors[2–4]. As a result of their acylation, Wnt proteins are very hydrophobic and require detergents for purification, which presents major obstacles to the preparation and application of recombinant Wnt proteins. This hydrophobicity has hindered the determination of the molecular mechanisms of Wnt signalling activation and the functional importance of FZD subtypes, and the use of Wnt proteins as therapeutic agents. Here we develop surrogate Wnt agonists, water-soluble FZD–LRP5/LRP6 heterodimerizers, with FZD5/FZD8-specific and broadly FZD-reactive binding domains. Similar to WNT3A, these Wnt agonists elicit a characteristic β-catenin signalling response in a FZD-selective fashion, enhance the osteogenic lineage commitment of primary mouse and human mesenchymal stem cells, and support the growth of a broad range of primary human organoid cultures. In addition, the surrogates can be systemically expressed and exhibit Wnt activity *in vivo* in the mouse liver, regulating metabolic liver zonation and promoting hepatocyte proliferation, resulting in hepatomegaly. These surrogates demonstrate that canonical Wnt signalling can be activated by bi-specific ligands that induce receptor heterodimerization. Furthermore, these easily produced, non-lipidated Wnt surrogate agonists facilitate functional studies of Wnt signalling and the exploration of Wnt agonists for translational applications in regenerative medicine.

The direct engagement of the Wnt lipid by the cysteine-rich domain (CRD) of FZD, and the extremely unusual fold of Wnt proteins[4] (Fig. 1a) presented a sub-optimal scaffold to re-engineer Wnt as a water-soluble protein, so we developed a strategy to engineer surrogate proteins that are structurally unrelated to Wnt proteins. While forced heterodimerization of genetically modified FZD, LRP5 and LRP6 (LRP5/LRP6) Wnt receptors can enhance signalling[5–8], it remains unclear whether intrinsic structural properties of Wnt, or natural ligands such as norrin (NDP), are required for normal canonical signalling, and whether dimerization alone by an engineered ligand would be sufficient for signalling activation. We engineered water-soluble Wnt agonists by linking antagonistic FZD and LRP5/LRP6-binding modules into a single polypeptide chain, thus forcing receptor heterodimerization while blocking endogenous Wnt binding (Fig. 1a). We used FZD subtype-specific and cross-reactive binding modules for restricted and broad cell-type specificity, respectively. For the FZD subtype-specific binder, through an integration of *de novo* design and protein engineering using yeast surface display, we created B12, a four-helix bundle domain protein derived from *Bacillus halodurans*, which binds specifically to the closely related FZD proteins FZD5 and FZD8, with relative affinities of 9 and 18 nM (Fig. 1a, b and Extended Data Figs 1, 2a–c). The crystal structure revealed that B12 binds FZD8 CRD at the rim of the lipid-binding groove engaging the FZD5/FZD8-specific Trp73 as hotspot residue. Leu56 and Leu61 in the loop following helix 2 bind to the groove, resulting in partial overlap with the Wnt lipid-binding site, and weak Wnt antagonism (Fig. 1c and Extended Data Fig. 2d). For the FZD cross-reactive analogue, we used the single-chain variable fragment (scFv) of the Wnt antagonizing antibody vantictumab, which binds FZD1, FZD2, FZD5, FZD7 and FZD8 with high affinity (0.7–1.4 nM)[9] (Fig. 1b and Extended Data Fig. 2e–h). To create FZD–LRP5/LRP6 heterodimerizers, we linked the FZD-binding modules (B12 and scFv) to the C-terminal domain of the human Wnt antagonist DKK1. This C-terminal domain, which is sufficient for Wnt inhibition and binds LRP5/LRP6 with moderate affinity (20–70 nM)[10,11], was linked to B12 and scFv through a flexible Gly-Ser polypeptide linker of 0–15 amino acids and 5 amino acids, respectively (these fusions are referred to as B12–DKK1c and scFv–DKK1c throughout) (Fig. 1a).

To interrogate whether the surrogates heterodimerize and cluster FZD and LRP5/LRP6 on live cell surfaces comparably to Wnts[11,12], we probed the assembly and diffusion dynamics of FZD8 and LRP6 upon the addition of Wnt proteins and surrogates by dual-colour single-molecule fluorescence imaging. FZD8 and LRP6 fused to an N-terminal SNAP-tag and HaloTag, respectively, were transiently expressed in HeLa cells and labelled with photostable fluorophores DY649 and tetramethylrhodamine (TMR), respectively[13] (Fig. 1d). IWP-2, an inhibitor of endogenous Wnt secretion, reduced the basal low levels of receptor co-localization (Extended Data Fig. 3a and Supplementary Video 1). After the addition of scFv–DKK1c, B12–DKK1c, *Xenopus* Wnt8 (XWnt8) and WNT3A, FZD8–LRP6 complexes with reduced mobility were detected by co-locomotion and single complex trajectories analysis (Fig. 1d, e, Extended Data Figs 3b, c, 4 and Supplementary Videos 2–5). In addition, the rates of FZD8–LRP6 dimerization and β-catenin accumulation induced by Wnt proteins and by surrogates correlate well (Extended Data Fig. 3d–j). Moreover, complexes with

[1]Department of Molecular and Cellular Physiology, Howard Hughes Medical Institute, and Department of Structural Biology, Stanford University School of Medicine, Stanford, California 94305, USA. [2]Department of Biochemistry, Howard Hughes Medical Institute, and the Institute for Protein Design, University of Washington, Seattle, Washington 98195, USA. [3]Division of Biophysics, Department of Biology, University of Osnabrück, 49076 Osnabrück, Germany. [4]Department of Medicine, Division of Hematology, Stanford University School of Medicine, Stanford, California 94305, USA. [5]Hubrecht Institute, Royal Netherlands Academy of Arts and Sciences, and University Medical Center Utrecht, Uppsalalaan 8, 3584 CT Utrecht, The Netherlands. [6]Program for Skeletal Disease and Tumor Microenvironment and Center for Cancer and Cell Biology, Van Andel Research Institute, 333 Bostwick NE, Grand Rapids, Michigan 49503, USA. [7]Hagey Laboratory for Pediatric Regenerative Medicine and Department of Surgery, Institute for Stem Cell Biology and Regenerative Medicine, Stanford University School of Medicine, Stanford, California 94305, USA. *These authors contributed equally to this work.

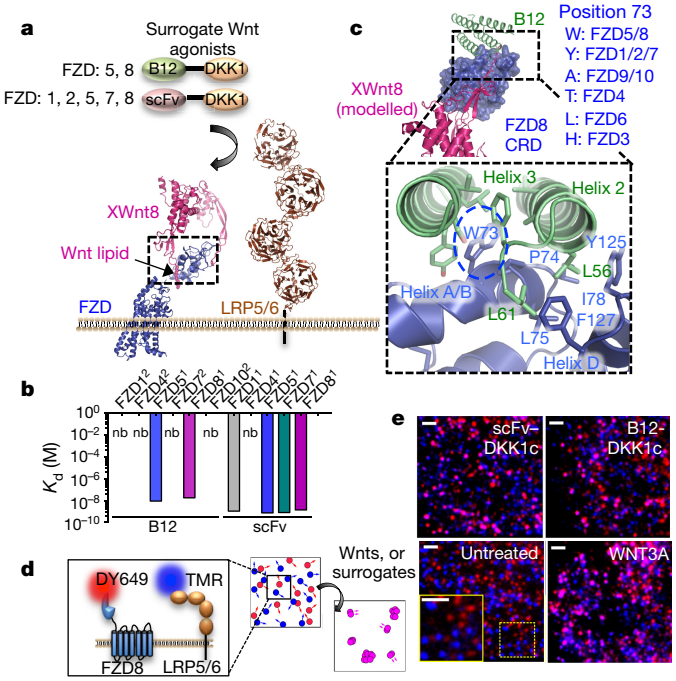

Figure 1 | Engineering of FZD-specific and cross-reactive LRP6–FZD heterodimerizers. a, Concept of Wnt surrogate-induced heterodimerization of FZD and LRP5 or LRP6. **b**, Binding affinities and specificities of B12 and scFv, determined by surface plasmon resonance (superscript 1), and yeast surface binding titration (superscript 2). nb, no binding. K_d, dissociation constant. **c**, Crystal structure of B12 (green) bound to FZD8 CRD (blue), with modelled binding of XWnt8 and Wnt lipid (purple). Zoomed-in view of the B12–FZD8 CRD binding interface, with side chains mediating critical contacts shown as sticks. Residues that substitute for Trp73 in different FZD proteins are listed. Crystallographic data and refinement statistics are summarized in Supplementary Table 1. **d**, **e**, Schematic representation (**d**) and typical single-molecule fluorescence images (**e**) for FZD8 (red) and LRP6 (blue) co-locomotion (magenta) mediated by scFv–DKK1c, B12–DKK1c and WNT3A in the plasma membrane of HeLa cells. Scale bars, 2 μm.

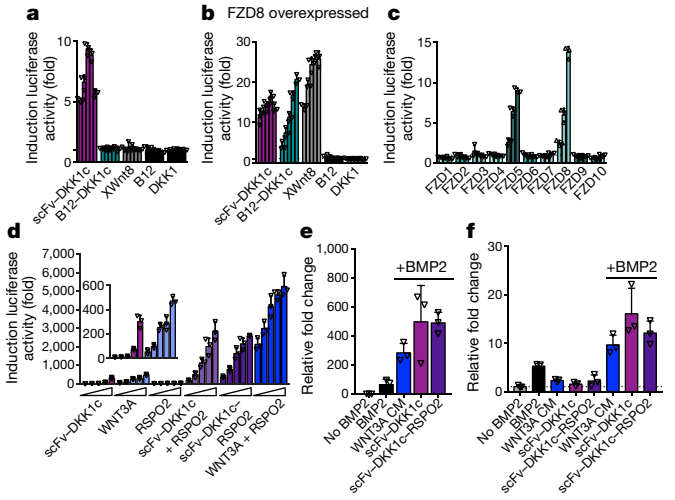

Figure 2 | FZD-specific activation of canonical Wnt signalling by Wnt surrogates. a, **b**, Activation of the β-catenin-dependent STF luciferase reporter by Wnt surrogates (scFv–DKK1c, B12–DKK1c), XWnt8 or negative control proteins (B12, DKK1) (3–50 nM) in mouse L cells (endogenously expressing FZD7) without (**a**) and with (**b**) overexpression of FZD8. **c**, Activation of the STF reporter by B12–DKK1c (5, 25, 100 nM) in L cells overexpressing the 10 mouse FZD receptors. **d**, RSPO2 (5–75 nM) potentiates the activity of scFv–DKK1c (5–75 nM) and WNT3A conditioned media (CM) (25–45%), as demonstrated by enhanced expression of the STF reporter in HEK293 cells. The scFv–DKK1c–RSPO2 fusion replicates the enhanced activity of the individual proteins. **e**, Upregulation of early osteogenic marker *Alpl* mRNA in mouse C3H10T1/2 cells treated for 4 days with WNT3A conditioned media, 50 nM scFv–DKK1c and 50 nM scFv–DKK1c–RSPO2 in the presence of 200 ng ml^{-1} BMP2 in osteogenic media. **f**, Upregulation of *ALPL* mRNA in human primary MSCs treated for 3 days with WNT3A conditioned media, 50 nM scFv–DKK1c and 50 nM scFv–DKK1c–RSPO2 in the presence and absence of 200 ng ml^{-1} BMP2. Error bars represent s.d. of $n = 3$ technical replicates from 1 of 3 (**a**–**c**, **e**, **f**) and 5 (**d**) representative experiments.

increased intensities were observed, confirming comparable FZD8 and LRP6 oligomerization by Wnt proteins and surrogates (Extended Data Fig. 5).

To determine whether the surrogate proteins elicited FZD-specific activation of canonical Wnt signalling, we performed a series of reporter assays. scFv–DKK1c, but not B12–DKK1c, XWnt8 or negative controls, activated Wnt signalling in mouse L cells (expressing FZD7), which can be sensitized to B12–DKK1c and XWnt8 by specifically overexpressing FZD5 or FZD8 (Fig. 2a–c and Extended Data Fig. 6a). Although Wnt signalling in human A375 and SH-SY5Y cells (expressing FZD2) was robustly induced only by scFv–DKK1c, both surrogates induced reporter expression in A549 cells (expressing FZD2, FZD4, FZD6 and FZD8) (Extended Data Fig. 6b–d). In agreement with their specificities, B12–DKK1c and scFv–DKK1c were antagonized by neutralizing (FZD8 CRD–Fc versus FZD1/FZD8 CRD–Fc) and blocking (isolated DKK1, B12 versus DKK1) domains (Extended Data Fig. 6e, f). Furthermore, scFv–DKK1c triggered LRP6 phosphorylation and accumulation of β-catenin in A375 cells, comparable to WNT3A conditioned media, characteristic of canonical Wnt pathway activation (Extended Data Fig. 6g). In addition, scFv–DKK1c and B12–DKK1c enhanced the transcription of the universal Wnt target gene *AXIN2* in SH-SY5Y and A549 cells, respectively, similar to control Wnt proteins (Extended Data Fig. 6h, i). Notably, B12–DKK1c with different linkers displays differential activity as reflected in signalling amplitudes (Extended Data Fig. 6i, j), demonstrating that the signal strength of the surrogate can be 'tuned' by variations in proximity of the binding modules. In HEK293 cells, RSPO2 strongly potentiates the activity of scFv–DKK1c, similar to WNT3A conditioned media[14] (Fig. 2d), adding further validation to the surrogates signalling in a 'Wnt-like' mechanism. Furthermore, a single-chain fusion protein consisting of RSPO2 linked to the C-terminal end of scFv–DKK1c replicates the enhanced activity of the combination (Fig. 2d).

Given that Wnt signalling has a pivotal role in bone formation[15], we evaluated the activity of the Wnt surrogates on mesenchymal stem cells (MSCs). scFv–DKK1c and scFv–DKK1c–RSPO2 enhanced the dose-dependent upregulation of the early osteogenesis marker alkaline phosphatase (*Alpl*) in mouse C3H10T1/2 multipotent MSCs (mRNA and enzymatic activity) (Extended Data Fig. 7a, b). In agreement with recent reports[16], WNT3A and Wnt surrogates synergize with BMP2 to enhance upregulation of alkaline phosphatase, while suppressing expression of BMP2-induced chondrogenesis marker collagen 2A1 (*Col2a1*) (Fig. 2e and Extended Data Fig. 7c, d). A synergistic upregulation of alkaline phosphatase was also observed in primary human MSCs (mRNA and enzymatic activity) and mouse MSCs (enzymatic activity) (Fig. 2f and Extended Data Fig. 7e–h), suggesting that the Wnt surrogates could be therapeutic candidates to enhance bone regeneration.

In the presence of the required niche factors, such as WNT3A and RSPO, adult stem cells can develop into 3D organoids that resemble their corresponding organs, recapitulating their regenerative capacity *ex vivo*[17–20]. To test whether scFv–DKK1c could substitute for WNT3A, we grew organoids from single-cell suspensions of normal human tissues in the presence or absence of recombinant scFv–DKK1c and scFv–DKK1c–RSPO2, and conditioned media from WNT3A, RSPO3 and IWP-2. Pancreas, stomach, colon and liver produce endogenous Wnt proteins, and organoids grow in the presence of RSPO3 and absence of exogenous Wnt, which is suppressed by IWP-2 (Fig. 3 and

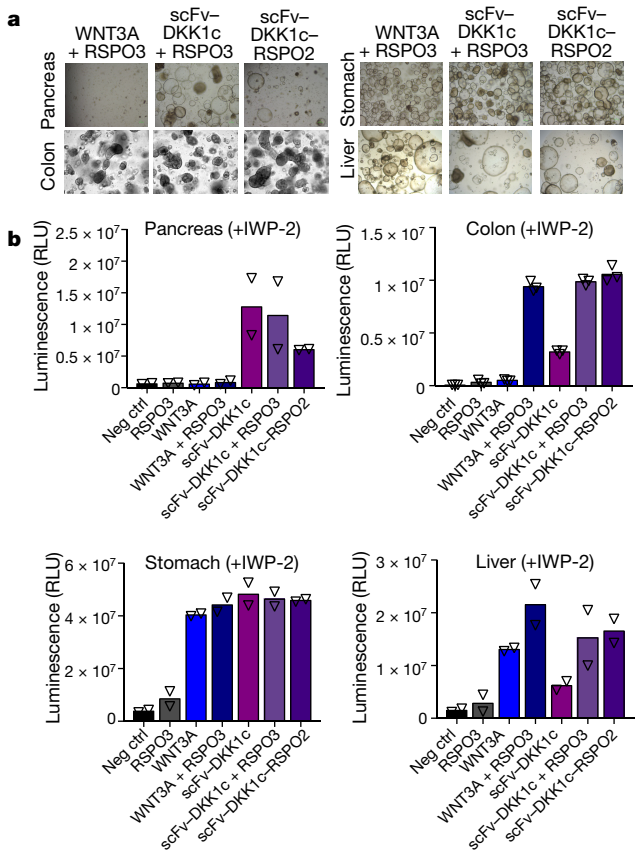

Figure 3 | Activity of Wnt surrogates on human organoid cultures *in vitro*. **a**, Representative bright-field images of organoids of human pancreas, colon, stomach (corpus) and liver, expanded for 12 days in basal media containing 3 μM IWP-2 and tissue-specific growth factors (Supplementary Table 2), and supplemented with 50% WNT3A and 2% RSPO3 conditioned media, 200 nM scFv–DKK1c plus 2% RSPO3 conditioned media, and 200 nM scFv–DKK1c–RSPO2. **b**, Quantification of cell proliferation and organoid expansion (live cells based on the presence of intracellular ATP in metabolically active cells) by luminescence. RLU, relative light units. Data are mean and s.d. from $n = 2$ (pancreas, liver and stomach) and 3 (liver) technical replicates, from 1 of 3 (colon), 2 (liver and pancreas) and 1 (stomach) representative experiments.

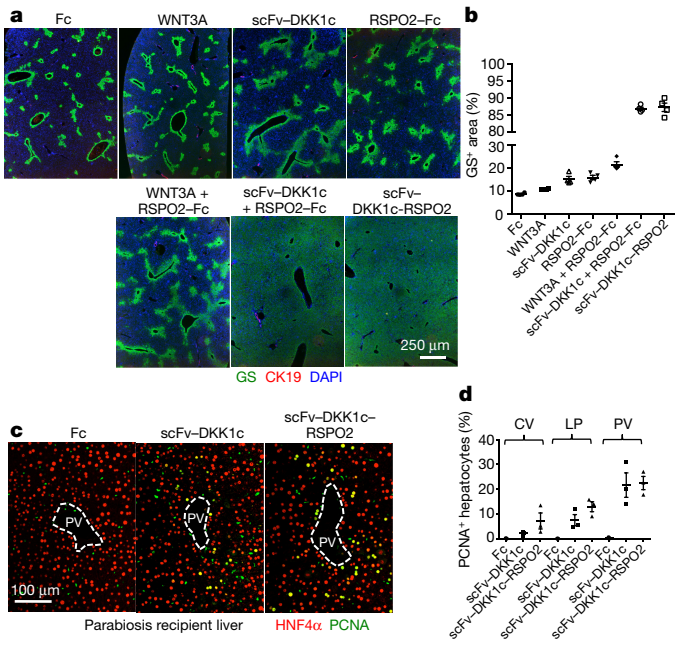

Figure 4 | Engineered Wnt surrogate is bioactive and upregulates Wnt signalling *in vivo*. **a**, Representative images of glutamine synthetase (GS; pericentral marker) and CK19 (bile duct/portal marker) immunofluorescence staining of livers from mice that received adenoviruses expressing the mouse IgG2α Fc fragment, mouse WNT3A, scFv–DKK1c, human RSPO2–Fc, WNT3A plus RSPO2–Fc, scFv–DKK1c plus RSPO2–Fc or scFv–DKK1c–RSPO2, 7 days after adenovirus injection ($n = 4$ mice per group). **b**, Quantification of the glutamine synthetase immunofluorescence staining area shown in **a** relative to liver tissue area, with vessel lumen area subtracted ($n = 4$ mice per group). **c**, **d**, Effects of scFv–DKK1c and scFv–DKK1c–RSPO2 on hepatocyte proliferation determined in surgically paired mice by parabiosis. The donor mice received adenoviruses intravenously 2 days before parabiosis surgery with recipient mice to establish cross-circulation and allow diffusion of the transgenes in both mice. Immunofluorescent staining (**c**) and quantification of proliferating hepatocytes (**d**) in recipient mice with PCNA and HNF4α 7 days after parabiosis surgery. CV, central vein; LP, liver parenchyma; PV, portal vein. $n = 3$ mice per group. Experiments demonstrating the regulation of liver zonation were performed at least twice for each condition ($n = 4$ mice per group); the parabiosis experiment was done once in the laboratory ($n = 3$ mice per group). Error bars represent s.e.m. from biological replicates.

Extended Data Fig. 8a–e). In the presence of IWP-2, scFv–DKK1c and scFv–DKK1c–RSPO2 were superior or comparable to WNT3A conditioned media in promoting the continuous growth of organoids derived from the pancreas, colon and stomach (corpus); however, they were less active in supporting the growth of liver organoids (Fig. 3 and Extended Data Fig. 8a–e). The differential activity might be attributed to differential FZD specificity and unknown factors in the conditioned media. Intestinal organoids represent a model for personalized cystic fibrosis drug screening[21]. While intestinal organoids from healthy donors swell upon the opening of cystic fibrosis transmembrane conductance regulator (CFTR) channels by cAMP, cystic fibrosis organoids will only swell when pretreated with CFTR-activating or -stabilizing drugs. Wnt surrogates supported the growth of strongly budded organoids, in a comparable manner to WNT3A (Extended Data Fig. 8f), yet they offer the opportunity to culture organoids in defined media, circumventing the interference of unknown components with the assay.

To assess the activities of Wnt surrogates *in vivo*, we used a recombinant adenoviral expression system to deliver scFv–DKK1c and scFv–DKK1c–RSPO2 systemically in mice. When injected intravenously, adenoviruses infect hepatocytes, resulting in durable expression of the transgenes[22]. In the liver, Wnt proteins are expressed around the central vein[23], and activate a Wnt-driven pericentral gene expression program, such as glutamine synthetase (encoded by *Glul* in mice, also known as *Gln*s), in hepatocytes immediately adjacent to the source, resulting in metabolic zonation[24]. We infected wild-type C67Bl/6J mice with adenoviruses expressing scFv–DKK1c (Ad-scFv–DKK1c), scFv–DKK1c–RSPO2 (Ad-scFv–DKK1c–RSPO2), mouse WNT3A (Ad-Wnt3a), human RSPO2–Fc fusion (Ad-RSPO2–Fc) or mouse IgG2α Fc fragment (Ad-Fc) as a negative control ($n = 4$ mice per group). Infection of the liver was confirmed by quantitative reverse transcription PCR (qRT–PCR), and circulating levels of scFv–DKK1c and scFv–DKK1c–RSPO2 proteins (Extended Data Fig. 9a–f), but not WNT3A (data not shown), were detected in the peripheral blood. After 7 days, Ad-scFv–DKK1c, Ad-RSPO2–Fc and Ad-Wnt3a modestly expanded the glutamine synthetase-expressing region, while repressing the periportal marker *Cyp2f2* (inhibited by Wnt pathway activation) and inducing *Axin2* mRNA compared to control mice (Fig. 4a, b and Extended Data Fig. 9g–i). Notably, Ad-scFv–DKK1c plus Ad-RSPO2–Fc, Ad-scFv–DKK1c–RSPO2, and to a lesser extent Ad-Wnt3a plus Ad-RSPO2–Fc elicited a synergistic induction of glutamine synthatase protein (in approximately 90% of the liver lobule) and *Axin2* mRNA expression, and suppression of *Cyp2f2* mRNA (Fig. 4a, b and Extended Data Fig. 9g–i).

To examine the effect of scFv–DKK1c or scFv–DKK1c–RSPO2 on hepatocyte proliferation, we infected adult C57Bl/6J donor mice with Ad-scFv–DKK1c, Ad-scFv–DKK1c–RSPO2 or Ad-Fc followed by

parabiosis in which the circulatory systems of two mice are conjoined (Extended Data Fig. 10a). Although scFv–*Dkk1c* and scFv–DKK1c-*Rspo2* mRNA were only detected in the livers of donor mice, serum scFv–DKK1c and scFv–DKK1c–RSPO2 proteins, enhanced liver expression of *Glul* and *Axin2*, and reduced liver expression of *Cyp2f2* were present in donor and recipient mice (Extended Data Fig. 10b–i), confirming that adenoviral infection was confined to the donor. The livers in recipient mice treated with scFv–DKK1c or scFv–DKK1c–RSPO2 exhibited mild hepatomegaly and markedly increased proliferation of HNF4α-positive hepatocytes in all hepatocyte zones, which was most pronounced in the periportal region, similar to recent observations with R-spondin[25] (Fig. 4c, d and Extended Data Fig. 10j). Therefore, these surrogates activate Wnt signalling *in vivo*, and alter Wnt-driven hepatic metabolic zonation and proliferation. Given the tight feedback regulation of the Wnt pathway, indirect effects cannot be entirely ruled out. Furthermore, an accompanying study[26] demonstrates that the Wnt surrogates induce proliferation of intestinal crypt cells, confirming their activity on tissues distant from the site of protein production.

The development of surrogate Wnt agonists offers both conceptual insight into Wnt signalling and a practical advance for experimental and therapeutic applications. The ability of the bi-specific heterodimerizer scFv–DKK1c, which concurrently blocks endogenous Wnt binding, to mimic Wnt activity demonstrates that the FZD and LRP5/LRP6 receptors follows the paradigm of signalling activation through receptor dimerization, as seen for growth factor and cytokine receptors[27,28]. The relative orientations and proximities of the receptors induced by Wnt ligands, and the surrogates, are probably the principle parameters determining the efficiency of signal initiation. However, we cannot rule out the possibility that natural Wnt ligands, and also the cysteine-knot growth factor norrin that also activates canonical Wnt signalling by FZD4 and LRP5/LRP6 oligomerization[29–31], may possess intrinsic structural features that initiate additional or alternative signalling outcomes, such as by inducing ligand-specific conformational changes in FZD and/or LRP5/6. Future experiments investigating the signalling and functional properties of Wnt proteins versus the surrogates will clarify such questions. The ease of Wnt surrogate production, and the ability of Wnt proteins to target specific FZD subtypes, may allow for a better control of Wnt and FZD pleiotropy, facilitating the introduction of Wnt agonism into the clinic for regenerative medicine applications.

Online Content Methods, along with any additional Extended Data display items and Source Data, are available in the online version of the paper; references unique to these sections appear only in the online paper.

Received 3 May 2016; accepted 27 March 2017.
Published online 3 May 2017.

1. Clevers, H. & Nusse, R. Wnt/β-catenin signaling and disease. *Cell* **149,** 1192–1205 (2012).
2. Willert, K. *et al.* Wnt proteins are lipid-modified and can act as stem cell growth factors. *Nature* **423,** 448–452 (2003).
3. Takada, R. *et al.* Monounsaturated fatty acid modification of Wnt protein: its role in Wnt secretion. *Dev. Cell* **11,** 791–801 (2006).
4. Janda, C. Y., Waghray, D., Levin, A. M., Thomas, C. & Garcia, K. C. Structural basis of Wnt recognition by Frizzled. *Science* **337,** 59–64 (2012).
5. Cong, F., Schweizer, L. & Varmus, H. Wnt signals across the plasma membrane to activate the beta-catenin pathway by forming oligomers containing its receptors, Frizzled and LRP. *Development* **131,** 5103–5115 (2004).
6. Holmen, S. L., Robertson, S. A., Zylstra, C. R. & Williams, B. O. Wnt-independent activation of beta-catenin mediated by a Dkk1–Fz5 fusion protein. *Biochem. Biophys. Res. Commun.* **328,** 533–539 (2005).
7. Liu, G., Bafico, A. & Aaronson, S. A. The mechanism of endogenous receptor activation functionally distinguishes prototype canonical and noncanonical Wnts. *Mol. Cell. Biol.* **25,** 3475–3482 (2005).
8. Mulligan, K. A. *et al.* Secreted Wingless-interacting molecule (Swim) promotes long-range signaling by maintaining Wingless solubility. *Proc. Natl Acad. Sci. USA* **109,** 370–377 (2012).
9. Gurney, A. *et al.* Wnt pathway inhibition via the targeting of Frizzled receptors results in decreased growth and tumorigenicity of human tumors. *Proc. Natl Acad. Sci. USA* **109,** 11717–11722 (2012).
10. Ahn, V. E. *et al.* Structural basis of Wnt signaling inhibition by Dickkopf binding to LRP5/6. *Dev. Cell* **21,** 862–873 (2011).
11. Bourhis, E. *et al.* Reconstitution of a Frizzled8·Wnt3a·LRP6 signaling complex reveals multiple Wnt and Dkk1 binding sites on LRP6. *J. Biol. Chem.* **285,** 9172–9179. (2010).
12. Bilic, J. *et al.* Wnt induces LRP6 signalosomes and promotes dishevelled-dependent LRP6 phosphorylation. *Science* **316,** 1619–1622 (2007).
13. Wilmes, S. *et al.* Receptor dimerization dynamics as a regulatory valve for plasticity of type I interferon signaling. *J. Cell Biol.* **209,** 579–593 (2015).
14. Hao, H. X. *et al.* ZNRF3 promotes Wnt receptor turnover in an R-spondin-sensitive manner. *Nature* **485,** 195–200 (2012).
15. Zhong, Z., Ethen, N. J. & Williams, B. O. WNT signaling in bone development and homeostasis. *Wiley Interdiscip. Rev. Dev. Biol.* **3,** 489–500 (2014).
16. Salazar, V. S., Ohte, S., Capelo, L. P., Gamer, L. & Rosen, V. Specification of osteoblast cell fate by canonical Wnt signaling requires Bmp2. *Development* **143,** 4352–4367 (2016).
17. Kretzschmar, K. & Clevers, H. Organoids: modeling development and the stem cell niche in a dish. *Dev. Cell* **38,** 590–600 (2016).
18. Sato, T. *et al.* Single Lgr5 stem cells build crypt-villus structures *in vitro* without a mesenchymal niche. *Nature* **459,** 262–265 (2009).
19. Barker, N. *et al.* $Lgr5^{+ve}$ stem cells drive self-renewal in the stomach and build long-lived gastric units *in vitro*. *Cell Stem Cell* **6,** 25–36 (2010).
20. Huch, M. *et al. In vitro* expansion of single $Lgr5^{+}$ liver stem cells induced by Wnt-driven regeneration. *Nature* **494,** 247–250 (2013).
21. Dekkers, J. F. *et al.* A functional CFTR assay using primary cystic fibrosis intestinal organoids. *Nat. Med.* **19,** 939–945 (2013).
22. Wei, K., Kuhnert, F. & Kuo, C. J. Recombinant adenovirus as a methodology for exploration of physiologic functions of growth factor pathways. *J. Mol. Med. (Berl.)* **86,** 161–169 (2008).
23. Wang, B., Zhao, L., Fish, M., Logan, C. Y. & Nusse, R. Self-renewing diploid $Axin2^{+}$ cells fuel homeostatic renewal of the liver. *Nature* **524,** 180–185 (2015).
24. Benhamouche, S. *et al.* Apc tumor suppressor gene is the "zonation-keeper" of mouse liver. *Dev. Cell* **10,** 759–770 (2006).
25. Planas-Paz, L. *et al.* The RSPO–LGR4/5–ZNRF3/RNF43 module controls liver zonation and size. *Nat. Cell Biol.* **18,** 467–479 (2016).
26. Yan, K. S. *et al.* Non-equivalence of Wnt and R-spondin ligands during $Lgr5^{+}$ intestinal stem-cell self-renewal. *Nature* http://dx.doi.org/10.1038/nature22313 (this issue).
27. Lemmon, M. A. & Schlessinger, J. Transmembrane signaling by receptor oligomerization. *Methods Mol. Biol.* **84,** 49–71 (1998).
28. Spangler, J. B., Moraga, I., Mendoza, J. L. & Garcia, K. C. Insights into cytokine-receptor interactions from cytokine engineering. *Annu. Rev. Immunol.* **33,** 139–167 (2015).
29. Xu, Q. *et al.* Vascular development in the retina and inner ear: control by Norrin and Frizzled-4, a high-affinity ligand-receptor pair. *Cell* **116,** 883–895 (2004).
30. Ke, J. *et al.* Structure and function of Norrin in assembly and activation of a Frizzled 4-Lrp5/6 complex. *Genes Dev.* **27,** 2305–2319 (2013).
31. Chang, T. H. *et al.* Structure and functional properties of Norrin mimic Wnt for signalling with Frizzled4, Lrp5/6, and proteoglycan. *eLife* **4,** (2015).

Supplementary Information is available in the online version of the paper.

Acknowledgements We thank the staff of the Advanced Light Source (ALS), Lawrence Berkeley National Laboratory, for support and access to beamline 8.2.2, and P. Chu from the Department of Comparative Medicine Animal Histology Service Center for sample preparation. This work was supported by National Institutes of Health (NIH) R01 GM097015 (to K.C.G), K08DK096048 (to K.S.Y), U01 DK085527 (to C.J.K.), U19 AI116484 (to C.J.K.), U01 CA176299 (to C.J.K.); DFG SFB 944 (to J.P.); Bu,rroughs Wellcome Fund CAMS (to K.S.Y.); the Stinehart/Reed Foundation (to K.C.G.); the Ludwig Foundation (K.C.G., C.J.K.); the Howard Hughes Medical Institute (to K.C.G., D.B.), the European Union's Horizon 2020 research and innovation program under grant agreement no. 668294 (to H.C.), and the NWO translational Adult Stem Cell Research grant 40-41400-98-1108 (to H.C.).

Author Contributions C.Y.J. designed experiments, performed biophysical measurements, determined crystal structures, performed *in vitro* functional assays and prepared the manuscript. D.S. analysed data. D.B., L.T.D. and J.D.M. designed the B12 binding module, and performed affinity maturation. J.P. and C.Y. performed TIRF microscopy, analysed data and contributed to manuscript preparation. Z.A.Z. and B.O.W. performed osteogenesis assays, and analysed data. W.d.L. and H.C. performed organoid culture assays, analysed data and contributed to manuscript preparation. J.C., K.S.Y. and X.L. carried out *in vivo* experiments in mice and analysed data. O.M. performed parabiosis surgery. C.J.K. designed and supervised *in vivo* experiments, analysed data and contributed to manuscript preparation. K.C.G. conceived of the project, analysed data, supervised execution of the project, and prepared the manuscript.

Author Information Reprints and permissions information is available at www.nature.com/reprints. The authors declare competing financial interests: details are available in the online version of the paper. Readers are welcome to comment on the online version of the paper. Publisher's note: Springer Nature remains neutral with regard to jurisdictional claims in published maps and institutional affiliations. Correspondence and requests for materials should be addressed to K.C.G. (kcgarcia@stanford.edu).

Reviewer Information *Nature* thanks W. DeGrado, Y. Jones and the other anonymous reviewer(s) for their contribution to the peer review of this work.

METHODS

Cell lines. HEK293 cells stably transfected with the STF plasmid encoding the firefly luciferase reporter under the control of a minimal promoter, and a concatemer of 7 LEF/TCF binding sites[32], were obtained from J. Nathans. Mouse L cells stably transfected with the STF plasmid and a constitutively expressed *Renilla* luciferase (control reporter) were obtained from C. Kuo. L cells transfected with a mouse WNT3A expression vector to produce conditioned media were obtained from the ATCC. A375, SH-SY5Y and A549 cells were stably transfected with the BAR plasmid encoding the firefly luciferase reporter under the control of a minimal prompter and a concatemer of 12 TCF/LEF binding sites and a constitutively expressed *Renilla* luciferase (control reporter) using a lentiviral-based approach[33]. All reporter cell lines were cultured in complete DMEM medium (Gibco) supplemented with 10% FBS, 1% penicillin, streptomycin, and L-glutamine (Gibco), at 37 °C and 5% CO_2 and cultured in the presence of antibiotics for selection of the transfected reporter plasmid. C3H10T1/2 cells were obtained from the ATCC. Human primary MSCs were obtained from Cell Applications, Inc. Mouse primary MSCs were obtained from Invitrogen. Cell lines have not been tested for mycoplasma contamination.

Protein constructs, expression and purification. The coding sequence of B12 containing a C-terminal 6×His-tag was cloned into the pET28 vector (Novagen) for bacterial cytoplasmic protein expression. Protein expression was performed in transformed BL21 cells, expression was induced with 0.7 mM IPTG at an $OD_{600\,nm}$ of 0.8 for 3–4 h. Cells were pelleted, lysed by sonication in lysis buffer (20 mM HEPES, pH 7.2, 300 mM NaCl, 20 mM imidazole), and soluble fraction was applied to Ni-NTA agarose (QIAGEN). After washing the resin with lysis buffer containing 500 mM NaCl, B12 was eluted with 300 mM imidazole, and subsequently purified on a Superdex 75 size-exclusion column (GE Healthcare) equilibrated in HBS (10 mM HEPES, pH 7.2, 150 nM NaCl).

XWnt8 was purified from a stably transfected *Drosophila* S2 cell line co-expressing XWnt8 and mouse FZD8 CRD–Fc described previously[4]. Cells were cultured in complete Schneider's medium (Thermo Fisher Scientific), containing 10% FBS and supplemented with 1% L-glutamine, penicillin and streptomycin (Gibco), and expanded in Insect-Xpress medium (Lonza). A complex of XWnt8 and FZD8 CRD–Fc was captured from the conditioned media on Protein A agarose beads (Sigma). After washing with 10 column volumes of HBS, XWnt8 was eluted with HBS containing 0.1% *n*-dodecyl-β-D-maltoside (DDM) and 500 mM NaCl, while the FZD8 CRD–Fc remained bound to the beads.

All other proteins were expressed in High Five (*Trichoplusia ni*) cells (Invitrogen) using the baculovirus expression system. To produce the B12-based surrogate, the coding sequences of B12, a flexible linker peptide comprising of 0, 1, 2 or 3 GSGSG-linker repeats, followed by the C-terminal domain of human DKK1 (residues 177–266), and a C-terminal 6×His-tag, were cloned into the pAcGP67A vector (BD Biosciences). To clone the scFv-based surrogate ligand, the sequence of the Vantictumab was retrieved from the published patent, reformatted into a scFv, and cloned at the N terminus of the surrogate variant containing the GSGSG linker peptide. To produce recombinant FZD CRD for crystallization, surface plasmon resonance measurements, SEC-MALS experiments and functional assays, the CRDs of human FZD1 (residues 113–182), human FZD4 (residues 42–161), human FZD5 (residues 30–150), human FZD7 (residues 36–163), human FZD8 (residues 32–151) and human FZD10 (residues 30–150), containing a C-terminal 3C protease cleavage site (LEVLFQ/GP), a biotin acceptor peptide (BAP)-tag (GLNDIFEAQKIEWHE) and a 6×His-tag were cloned into the same vector. The human FZD8 CRD used for crystallization contained only a C-terminal 6×His-tag, in addition to a Asn49Gln mutation to mutate the *N*-linked glycosylation site. FZD1/FZD8 CRD for inhibition assay contained a C-terminal 3C protease cleavage site, Fc-tag (constant region of human IgG), and a 6×His-tag. Human DKK1 (residues 32–266) with a C-terminal BAP-tag and 6×His-tag, and the two furin-like repeats of human RSPO2 (residues 36–143) with a N-terminal Fc-tag and a C-terminal 6×His-tag, were cloned also into the pAcGP67A vector. All proteins were secreted from High Five insect cells grown in Insect-Xpress medium, and purified using Ni-NTA affinity purification, and size-exclusion chromatography equilibrated in HBS (10 mM HEPES, pH 7.3, 150 nM NaCl). Enzymatic biotinylation was performed in 50 mM bicine, pH 8.3, 10 mM ATP, 10 mM magnesium acetate, 0.5 mM D-biotin with recombinant glutathione *S*-transferase (GST)-tagged BirA ligase overnight at 4 °C, and proteins were subsequently re-purified on a Superdex 75 size-exclusion column to remove excess biotin.

Computational design of FZD8-specific binding domain. We attempted to mimic the native Wnt–FZD lipid–protein interaction with a *de novo* designed protein–protein binding interface. A 13-residue alanine helix was docked against the lipid-binding cleft using Foldit[34]. This structural element was grafted onto a diverse set of native helical proteins using the Rosetta Epigraft[35] application to discover scaffolds with compatible, shape-complementary backbones. Prototype designs were selected by interface size and optimized using RosettaScripts[36] to perform side-chain redesign. 50 selected designs were further manually designed to ensure charge complementarity and non-essential mutations were reverted to the wild-type amino acid identity to maximize stability. DNA was obtained from Gen9 and screened for binding via yeast surface display as previously described with 1 μM biotinylated FZD8 CRD pre-incubated with 025 μM SAPE (Life Technologies)[37]. A design based on the scaffold with PDB code 2QUP, a uncharacterized four-helix bundle protein from *Bacillus halodurans*, demonstrated binding activity under these conditions, whereas knockout mutants Ala52Arg and Ala53Asd made using the Kunkel method[38] abrogated binding, verifying that the functional interface used the predicted residues. Wild-type scaffold 2QUP did not bind, confirming that activity was specifically due to design.

Affinity maturation of B12. To improve the affinity of the original design, a full-coverage site-saturation mutagenesis library was constructed for design based on the 2QUP scaffold via the Kunkel mutagenesis method[38] using forward and reverse primers containing a 'NNK' degenerate codon and 21-bp flanking regions (IDT). A yeast library was transformed as previously described[39] and sorted for three rounds, collecting the top 1% of binders using the BD Influx cell sorter. Naive and selected libraries were prepared and sequenced, and the data was processed as previously described[37] using a Miseq (Illumina) according to manufacturer protocols. The most enriched 11 mutations were identified by comparison of the selected and unselected pools of binders and were combined in a degenerate library containing all enriched and wild-type amino acid identities at each of these positions. This combination library was assembled from the oligonucleotides (IDT) listed below for a final theoretical diversity of around 800 k distinct variants. This library was amplified, transformed, and selected to convergence over five rounds, yielding the optimized variant B12.

Ultramer1_fwd_164bp 5′-GCTAGTGGTGGAGGAGGCTCTGGTGGAGGCGGTAGCGGAGGCGGAGGGTCGGCTAGCCATATGGGCGTGAGCTTTAGCGAAGTGATGGGCAAACAGAAAGATGAACAGGCGCGTGAACAGCTGAAAGAAGGCATGAWAAAAATTGAAGAACAGGGCAAAAAGCT-3′; Ultramer2_rev_133bp 5′-AGCCACGACGTTCTTCCAGATTCKKTCCCAGAAAACCCGCCKSCRMCGCAAAARBCGCCACCGCTGCGRCATATTTCTGCAGCTCTTCCTGGGTACGGGTTTCGCTCAGCTTTTTGCCCTGTTCTTCAATTTT-3′; Ultramer3_fwd_147bp 5′-AATCTGGAAGAACGTCGTGGCTTTAATCGTCGGGGCAAAGAAGAAATTGGCAAAATTAGCGGAGAAGTGTACMWAAAACTGTTAGACCTGAAAAAAGCGGTGCGTGCGAAAGAAAAAAAGGGACTGGAATATTCTGAATATGGTGGGC-3′; Ultramer4_rev_128bp 5′-GTTGTTATCAGATCTCTATTACAAGTCCTCTTCAGAAATAAGCTTTTGTTCGGATCCGCCCCCCTCGAGCGCAKRAMYACKCTCCAGGRKGCCCTTAATCTCGCCCACCATATTCAGAATATCCAGTC-3′.

Complex crystallization and structure determination. The B12–FZD8 CRD(N49Q) complex was formed by mixing purified B12 and FZD8 CRD(N49Q) in stoichiometric quantities. The complex was then treated with 1:100 (w/w) carboxypeptidase A (Sigma) overnight at 4 °C, and purified on a Superdex 75 (GE Healthcare Life Sciences) size-exclusion column equilibrated in HBS. Purified complex was concentrated to around 15 mg ml^{-1} for crystallization trials. Crystals were grown by hanging-drop vapour diffusion at 295 K, by mixing equal volumes of the complex and reservoir solution containing 42–49% PEG 400, 0.1 M Tris, pH 7.8–8.2, 0.2 M NaCl, or 20% PEG 3000, 0.1 M sodium citrate, pH 5.5. While the PEG 400 condition is already a cryo-protectant, the crystals grown in the PEG 3000 condition were cryoprotected in reservoir solution supplemented with 20% glycerol before flash freezing in liquid nitrogen. Crystals grew in space groups $P2_1$ (PEG 400 condition) and $P2$ (PEG 3000 condition), respectively, with 2 and 4 complexes in the asymmetric units. Cell dimensions are listed in Supplementary Table 1. Data were collected at beamline 8.2.2 at the Advanced Light Source (ALS), Lawrence Berkeley National Laboratory. All data were indexed, integrated, and scaled with the XDS package[40]. The crystal structures in both space groups were solved by molecular replacement with the program PHASER[41] using the structure of the FZD8 CRD (PDB code 1IJY) and the designed model of a minimal core of B12 as search models. Missing residues were manually build in COOT[42] after initial rounds of refinement. Several residues at the N terminus (residues 1 to 16/17/20/21), at the C terminus (residues after 117) and several residues within loop regions were unstructured and could not been modelled. Furthermore, we observed that in both crystal forms, B12 underwent domain swapping, and one B12 molecule lent helix 3 and 2 to another B12, resulting in a closely packed B12 homodimer. The density of the loops connecting helixes 1 and 2, and 3 and 4 were clearly visible, and folded into helical turns. Yet, SEC-MALS experiments confirmed that B12 existed as a monomer in solution, and complexed FZD8 CRD with a 1:1 stoichiometry. PHENIX Refine[43] was used to perform group coordinate refinement (rigid body refinement), followed by individual coordinate refinement using gradient-driven minimization applying stereo-chemical restraints, NCS

restraints, and optimization of X-ray/stereochemistry weight, and individual B-factor refinement. Initial rounds of refinement were aided by restraints from the high-resolution mouse FZD8 CRD structure as a reference model. Real space refinement was performed in COOT into a likelihood-weighted SigmaA-weighted $2mF_o - DF_c$ map calculated in PHENIX. The final model in the $P2$ space group was refined to 3.20 Å with R_{work} and R_{free} values of 0.2002 and 0.2476, respectively (Supplementary Table 1). The quality of the structure was validated with MolProbity[44]. 99.5% of residues are in the favoured region of the Ramachandran plot, and no residue in the disallowed region. The structure within the $P2_1$ space group was refined to 2.99 Å with R_{work} and R_{free} values of 0.2253 and 0.2499, respectively, with 99.2% of residues in the favoured region of the Ramachandran plot, and no residues in the disallowed region. See Supplementary Table 1 for data and refinement statistics. Structure figures were prepared with the program PYMOL.

Affinity measurements of B12 and scFv–DKK1c interaction with FZD CRDs. Binding measurements were performed by surface plasmon resonance on a BIAcore T100 (GE Healthcare) and all proteins were purified on SEC before experiments. Biotinylated FZD1 CRD, FZD5 CRD, FZD7 CRD and FZD8 CRD were coupled at a low density to streptavidin on a SA sensor chip (GE Healthcare). An unrelated biotinylated protein was captured at equivalent coupling density to the control flow cells. Increasing concentrations of B12 and scFv–DKK1c were flown over the chip in HBS-P (GE Healthcare) containing 10% glycerol and 0.05% BSA at 40 µl ml^{-1}. The chip surface was regenerated after each injection with 2 M $MgCl_2$ in HBS-P or 50% ethylene glycol in HBS-P (scFv–DKK1c measurements), or 4 M $MgCl_2$ in HBS-P (B12 measurements) for 60 s. Curves were reference-subtracted and all data were analysed using the Biacore T100 evaluation software version 2.0 with a 1:1 Langmuir binding model to determine the K_d values.

Analysis of yeast displayed B12 binding to human FZD CRDs. To characterize the FZD-specificity of B12, the yeast display vector encoding B12 was transformed into EBY100 yeast. To induce the display of B12 on the yeast surface, cells were growing in SGCAA medium[45,46] for 2 days at 20 °C. 1×10^6 yeast cells per condition were washed with PBE (PBS, 0.5% BSA, 2 mM EDTA), and stained separately with 0.06–1,000 nM biotinylated FZD1/4/5/7/8/10 CRDs for 2 h at 4 °C. After washing twice with ice-cold PBE, bound FZD CRDs were labelled with 10 nM strepdavidin-Alexa647 for 20 min. Cells were fixed with 4% paraformaldehyde, and bound FZD CRD was analysing on an Accuri C6 flow cytometer.

Plasmids, cell culture and cell labelling for single-molecule fluorescence microscopy. FZD8 fused to an N-terminal HaloTag[47] and LRP6 fused to an N-terminal SNAP-tag[48] were cloned into the pSEMS-26m vector (Covalys Biosciences) by cassette cloning[49,50]. The template pSEMS-26m vectors had been coded with DNA sequences of the SNAP-tag or the HaloTag, respectively, together with an Igκ leader sequence (from the pDisplay vector, Invitrogen) as described previously[50]. The genes of full-length mouse *Fzd8* or human *LRP6* without the N-terminal signal sequences were inserted into pSEMS-26m via the XhoI and AscI or AscI and NotI, restriction sites, respectively. A plasmid encoding a model transmembrane protein, maltose-binding protein fused to a transmembrane domain, fused to an N-terminal HaloTag was prepared as described recently[13]. HeLa cells were cultivated at 37 °C, 5% CO_2 in MEM Earle's (Biochrom AG, FG0325) supplemented with 10% fetal calf serum and 1% nonessential amino acids. Cells were plated in 60-mm cell culture dishes to a density of 50% confluence and transfected via calcium phosphate precipitation[49]. 8–10 h after transfection, cells were washed twice with PBS and the medium was exchanged, supplied with 2 µM porcupine inhibitor IWP-2 for inhibiting maturation of endogenous Wnt in HeLa cells[51]. 24 h after transfection, cells were plated on glass coverslips pre-coated with PLL-PEG-RGD[52] for reducing nonspecific binding of dyes during fluorescence labelling. After culturing for 12 h, coverslips were mounted into microscopy chambers for live-cell imaging. SNAP-tag and HaloTag were labelled by incubating cells with 50 nM benzylguanine-DY649 (SNAP-Surface 649, New England Biolabs) and 80 nM of HaloTag tetramethylrhodamine ligand (HTL-TMR, Promega) for 20 min at 37 °C. Under these conditions, effective degrees of labelling estimated from single molecule assays with a HaloTag–SNAP-tag fusion protein were ~40% for the SNAP-tag and ~25% for the HaloTag[13]. After washing three times with PBS, the chamber was refilled with MEM containing 2 µM IWP-2 for single-molecule fluorescence imaging.

Single-molecule fluorescence microscopy. Single-molecule fluorescence imaging was carried out by using an inverted microscope (Olympus IX71) equipped with a triple-line total internal reflection (TIR) illumination condenser (Olympus) and a back-illuminated EMCCD camera (iXon DU897D, 512 × 512 pixel from Andor Technology). A 561-nm diode solid state laser (CL-561-200, CrystaLaser) and a 642-nm laser diode (Luxx 642-140, Omicron) were coupled into the microscope for excitation. Laser lights were reflected by a quad-line dichroic beam splitter (Di R405/488/561/647, Semrock) and passed through a TIRF objective (UAPO 150×/1.45, Olympus). For simultaneous dual-colour detection, a DualView microimager (Optical Insight) equipped with a 640 DCXR dichroic beamsplitter (Chroma) in combination with bandpass filters FF01-585/40 and FF01 670/30 (Semrock), respectively, was mounted in front of the camera. The overlay of the two channels was calibrated by imaging fluorescent microbeads (TetraSpeck microspheres 0.1 µm, T7279, Invitrogen), which were used for calculating a transformation matrix. After channel alignment, the deviation between the channels was below 10 nm.

For single-molecule imaging, typical excitation powers of 1 mW at 561 nm and 0.7 mW at 642 nm measured at the objective were used. Time series of 150–300 frames were recorded at 30 Hz (4.8–9.6 s). An oxygen scavenging system containing 0.5 mg ml^{-1} glucose oxidase, 40 mg ml^{-1} catalase, and 5% (w/v) glucose, together with 1 µM ascorbic acid and 1 µM methyl viologene, was added to minimize photobleaching[53]. Receptor dimerization was initiated by incubating with 100 nM Wnt proteins or surrogates. Images were acquired after 5 min incubation in the presence of the ligands. All live-cell imaging experiments were carried out at room temperature.

Receptor heterodimerization analysis. A 2D Gaussian mask was used for localizing single emitters[54,55]. For colocalization analysis to determine the heterodimerization fraction, particle coordinates from two channels were aligned by a projective transformation (*cp2tform* of type 'projective', MATLAB 2012a) according to the transformation matrix obtained from microbead calibration measurement. Particles colocalized within a distance of 150 nm were selected. Only co-localized particles, which could be tracked for at least 10 consecutive frames (that is, molecules co-locomoting for at least 0.32 s) were accepted as receptor heterodimers or hetero-oligomers, which has been previously found to be a robust criterion for protein dimerization[13]. The fraction of heterodimerization or hetero-oligomerization was determined as the number of co-locomotion trajectories with respect to the number of the receptor trajectories. Since the receptor expression level of FZD8 or LRP6 was variable in the transiently transfected cells, only cells with similar receptor expression levels were considered (less than three times the excess of one subunit over the other). The smaller number of trajectories of either FZD8 or LRP6 was regarded as the limiting factor and therefore taken as a reference for calculating the heterodimerized/hetero-oligomerized fraction. Oligomerization values were not corrected for the degree of labelling.

Single-molecule tracking. Single-molecule trajectories were reconstructed using the multi-target tracing (MTT) algorithm[56]. The detected trajectories were evaluated with respect to their step length distribution to determine the diffusion coefficients. For a reliable quantification of local mobilities, we estimated diffusion constants from the displacements with three frames (96 ms). Step-length histograms were obtained from all single molecule trajectories and fitted by a two-component model of Brownian diffusion, thus taking into account the intrinsic heterogeneity of protein diffusion in the plasma membrane[57,58]. A bimodal probability density function $p(r)$ was used for a nonlinear least square fit of the step-length histogram:

$$p(r) = \sum_i \alpha_i \cdot \frac{r}{\sigma_i^2} e^{(-r^2/2\sigma_i^2)} \text{ and } \sum_i \alpha_i = 1 \quad (1)$$

where α_i is the percentage of the fraction, $\sigma_i^2 = 2D_i n\delta t$ contains the diffusion coefficient of each fraction ($n\delta t = 96$ ms). Average diffusion coefficients were determined by weighting the diffusion coefficients with the corresponding fractions.

Single-molecule intensity assay. Single-molecule intensity distribution of individual diffraction-limited spots was extracted from the first 50 images of the recorded time lapse image sequence, in which photobleaching of dyes was kept below 10%[13]. Oligomerization of receptors was evaluated by fitting the obtained single molecule intensity with a multi-component Gaussian distribution function[59]. To ensure a reliable analysis, monomeric receptors were first distinguished based on the observation that monomers diffused much faster than oligomers. Therefore, the characteristic intensity distribution of monomeric receptor subunits was obtained by tracking of the fast mobile fraction. Fractions of the monomer, dimer, trimer and higher oligomers were then de-convoluted from the single molecule intensity distribution, presuming that intensities of clusters were multiples of the monomer intensity distribution.

STF and BAR luciferase reporter assays. Immortal cells were seeded in triplicate for each condition in 96-well plates, and stimulated with surrogates, XWnt8, WNT3A conditioned media, control proteins, or other treatments for 20–24 h. After washing cells with PBS, cells in each well were lysed in 30 µl passive lysis buffer (Promega). 10 µl per well of lysate was assayed using the Dual Luciferase Assay kit (Promega) and normalized to the *Renilla* luciferase signal driven constitutively by the human elongation factor-1 alpha promoter to account for cell

variability. A375 BAR, SH-SY5Y BAR, L STF and HEK293 STF cells were plated at a density of 10,000–20,000 cells per well, and treatment was started after 24 h in fresh medium. A549 BAR cells were plated at a density of 5,000 cells per well in the presence of 2 μM IWP-2 (Calbiochem) to suppress endogenous Wnt secretion, and treatment was started after 48 h in fresh medium containing fresh IWP-2.

β-catenin stabilization and LRP6 phosphorylation assay. To induce β-catenin accumulation, SH-SY5Y BAR cells were treated for 2 h with scFv–DKK1c, WNT3A conditioned media (positive control), B12 (negative control protein) and mock conditioned media (from untransfected L cells, negative control) at 37 °C, 5% CO_2. After, cells were washed twice with PBS. For β-catenin stabilization assay, cells were scraped into hypotonic lysis buffer (10 mM Tris-HCl pH 7.4, 0.2 mM $MgCl_2$, supplemented with protease inhibitors), incubated on ice for 10 min, and homogenized using a hypodermic needle. Sucrose and EDTA were added to final concentration of 0.25 M and 1 mM, respectively. For LRP6 phosphorylation assay, cells were lysed in RIPA buffer (50 mM Tris pH 8.0, 150 mM NaCl, 0.5% sodium deoxylate, 1% Triton X-100), supplemented with protease inhibitor and phosphatase inhibitor for 1 h at 4 °C. Lysates were centrifuged at 12,000*g* for 1 h at 4 °C. Supernatants were then diluted into SDS sample buffer. For immunoblotting, samples were resolved on a 12% Mini-PROTEAN(R)TGX precast protein gel (Bio-Rad) and transferred to a PVDF membrane. The membranes were cut horizontally approx. at the 64 kDa mark of the SeeBlue plus 2 molecular mass marker (Invitrogen). Top half of the blot was incubated with anti-β-catenin primary antibody ((D10A8)XP, rabbit, Cell Signaling 8480), LRP6 antibody ((C47E12), rabbit, Cell Signaling 3395), and P-LRP6 (S1490) antibody (rabbit, Cell Signaling 2568), and the bottom part with the anti-α-tubulin primary antibody (mouse, DM1A, Sigma) in PBS containing 0.1% Tween-20 and 5% BSA overnight at 4 °C. Blots were then washed, incubated with the corresponding secondary antibodies in the same buffer, before washing and developing using the ECL prime western blotting detection reagent (GE Healthcare).

Kinetic measurements of β-catenin accumulation. To induce β-catenin accumulation, K562 and cells were stimulated for 0, 15, 30, 45, 60, 90 and 120 min with 10 nM scFv–DKK1c, recombinant Wnt3a (R&D Systems), B12 (negative control protein) or plain complete growth medium at 37 °C, 5% CO_2. After, cells were washed twice with PBS, fixed with 4% PFA for 10 min at room temperature, and permeabilized in 100% methanol for at least 30 min at −80 °C. The cells were than stained with Alexa-647 conjugated anti-β-catenin antibody (L54E2) (Cell Signaling Technology, 1:100–1: 50 dilution). Fluorescence was analysed on an Accuri C6 flow cytometer.

RNA isolation, cDNA synthesis, and qPCR. Total RNA was isolated using either TRIZOL (Invitrogen) or RNeasy plus micro kit (QIAGEN) according to manufacturer's protocols. A total of 2 μg RNA were used to generate cDNA using the RevertAid RT kit (Life Technologies) using oligo(dT)18 mRNA primers (Life Technologies) according to manufacturer's protocol. 12 ng of cDNA per reaction were used. qPCR was performed using SYBR Green-based detection (Applied Biosystems) according to the manufacturer's protocol on a StepOnePlus real-time PCR system (ThermoFisher Scientific). All primers were published, or validated by us. Transcript copy numbers were normalized to GAPDH for each sample, and fold induction compared to control was calculated.

The following gene-specific validated primers were used: human *FZD1*: F: 5′-ATCCTGTGTGCTCCTCTTTTGG-3′, R: 5′-GATTGCTTTTCTCCTCTTCTTCAC-3′; human *FZD2*: F: 5′-CTGGGCGAGCGTGATTGT-3′, R: 5′-GTGGTGACAGTGAAGAAGGTGGAAG-3′; human *FZD3*: F: 5′-TCTGTATTTTGGGTTGGAAGCA-3′, R: 5′-CGGCTCTCATTCACTATCTCTTT-3′; human *FZD4*: F: 5′-TGGGCACTTTTTCGGTATTC-3′, R: 5′-TGCCCACCAACAAAGACATA-3′; human *FZD5*: F: 5′-CCATGATTCTTTAAGGTGAGCTG-3′, R: 5′-ACTTATTCAAGACACAACGATGG-3′; human *FZD6*: F: 5′-CGATAGCACAGCCTGCAATA-3′, R: 5′-ACGGTGCAAGCCTTATTTTG-3′; human *FZD7*: F: 5-TACCATAGTGAACGAAGAGGA-3′, R: 5′-TGTCAAAGGTGGGATAAAGG-3′; human *FZD8*: F: 5′-ACCCAGCCCCTTTTCCTCCATT-3′, R: 5′-GTCCACCCTCCTCAGCCAAC-3′; human *FZD9*: F: 5′-GCTGTGACTGGAATAAACCCC, R: 5′-GCTCTGCTTACAAGAAAGACTCC-3′; human *FZD10*: F: 5′-CTCTTCTCTGTGCTGTACACC, R: 5′-GTCTTGGAGGTCCAAATCCA-3′; mouse *Fzd1*: F: 5′-GCGACGTACTGAGCGGAGTG, R: 5′-TGATGGTGCGGATGCGGAAG-3′[60]; mouse *Fzd2*: F: 5′-CTCAAGGTGCCGTCCTATCTCAG, R: GCAGCACAACACCGACCATG-3′[60]; mouse *Fzd3*: F: 5′-GGTGTCCCGTGGCCTGAAG-3′, R: 5′-ACGTGCAGAAAGGAATAGCCAAG-3′[60]; mouse *Fzd4*: F: 5′-GACAACTTTCACGCCGCTCATC-3′, R: 5′-CAGGCAAACCCAAATTCTCTCAG-3′[60]; mouse *Fzd5*: F: 5′-AAGCTGCCTTCGGATGACTA-3′, R: 5′-TGCACAAGTTGCTGAACTCC-3′[60]; mouse *Fzd6*: F: 5′-TGTTGGTATCTCTGCGGTCTTCTG-3′, R: 5′-CTCGGCGGCTCTCACTGATG-3′[60]; mouse *Fzd7*: F: 5′-ATATCGCCTACAACCAGACCATCC-3′, R: 5′-AAGGAACGGCACGGAGGAATG-3′[60]; mouse *Fzd8*: F: 5′-GTTCAGTCATCAAGCAGCAAGGAG-3′, R: 5′-AAGGCAGGCGACAACGACG-3′[60]; mouse *Fzd9*: F: 5′-ATGAAGACGGGAGGCACCAATAC-3′, R: 5′-TAGCAGACAATGACGCAGGTGG-3′[60]; mouse *Fzd10*: F: 5′-ATCGGCACTTCCTTCATCCTGTC-3′, R: 5′-TCTTCCAGTAGTCCATGTTGAG-3′[60]; human *AXIN2*: F: 5′-CTCCCCACCTTGAATGAAGA-3′, R: 5′-TGGCTGGTGCAAAGACATAG-3′; human *GAPDH*: F: 5′-TGAAGGTCGGAGTCAACGGA-3′, R: 5′-CCATTGATGACAAGCTTCCCG-3′; mouse *Gapdh*: F: 5′-CCCCAATGTGTCCGTCGTG-3′, R: 5′-GCCTGCTTCACCACCTTCT-3′.

Osteogenic differentiation assay. Differentiation of C3H10T1/2, and human and mouse primary MSCs were performed essentially as described previously[61]. In brief, approximately 10,000 cells cm^{-2} were plated in normal culture medium (αMEM + FBS + penicillin/streptomycin), and allowed to adhere overnight. The following day, the medium was replaced with osteogenic medium (αMEM, 10% FBS, 1% penicillin/streptomycin, 50 μg ml^{-1} ascorbic acid, 10 mM β-glycerol phosphate (βGP), and replaced every other day. To determine alkaline phosphatase enzymatic activity, cells were fixed for 10 min with 10% formalin in PH7 PBS, before incubation in NBT-BCIP solution (1-Step(tm) NBT/BCIP Substrate Solution (Thermo Fisher Scientific, 34042) for 30 min. qPCR reactions were done with the SYBR method using the following primers: human *ACTB* F: 5′-GTTGTCGACGACGAGCG-3′, R: 5′-GCACAGAGCCTCGCCTT-3′; human *ALPL*: F: 5′-GATGTGGAGTATGAGAGTGACG-3′, R: 5′-GGTCAAGGGTCAGGAGTTC-3′; mouse *Alpl*: F: 5′-AAGGCTTCTTCTTGCTGGTG-3′, R: 5′-GCCTTACCCTCATGATGTCC-3′; mouse *Actb*: F: 5′-GGAATGGGTCAGAAGGACTC-3′, R: 5′-CATGTCGTCCCAGTTGGTAA-3′; mouse *Col2a1* F: 5′-GTGGACGCTCAGGAGAAACA-3′, R: 5′-TGACATGTCGATGCCAGGAC-3′.

Human organoid culture assay. P26N, normal adult human colon organoids, were established from a tumour-free colon segment of a patient diagnosed with CRC as described[18,62,63]. CFTR-derived colorectal organoids were obtained from a patient at Wilhelmina Children's Hospital WKZ-UMCU. Informed consent for the generation and use of these organoids for experimentation was approved by the ethical committee at University Medical Center Utrecht (UMCU) (TcBio 14-008). Human stomach organoids, derived from normal corpus and pylorus, were from patients that underwent partial or total gastrectomy at the University Medical Centre Utrecht (UMCU) and were established as described[19,64,65]. Pancreas organoids were obtained from the healthy part of the pancreas of patients undergoing surgical resection of a tumour at the University Medical Centre Utrecht Hospital (UMC) and were established as described[66,67]. The liver organoids were derived from freshly isolated normal liver tissue from a patient with metastatic CRC who presented at the UMC hospital (ethical approval code TCBio 14-007) and were established as described[20,68].

For the performance of 3D cultures, Matrigel (BD Biosciences) was used and overlaid with a liquid medium consisting of DMEM/F12 advanced medium (Invitrogen), supplemented with additional factors as outlined below. 2% RSPO3-CM (produced via the r-PEX protein expression platform at U-Protein Express BV), WNT3A conditioned medium (50%, produced using stably transfected L cells in the presence of DMEM/F12 advanced medium supplemented with 10% FBS), and Wnt and Wnt/RSPO2 surrogates at different concentrations were added as indicated. Single-cell suspensions of normal human organoids were cultured in duplicate or triplicate in round-bottom 96-well plates to perform a cell viability test using Cell Titer-Glo 3D (Promega). In brief, organoids were trypsinized to single-cell suspension and plated in 100 μl medium in the presence of the different reagents. 3 μM IWP-2 was added to inhibit endogenous Wnt lipidation and secretion. After 12 days, 100 μl of Cell Titer-Glo 3D was added, plates were shaken for 5 min, incubated for an additional 25 min and centrifuged before luminescence measurement.

***In vivo* experiments.** All animal experiments were conducted in accordance with procedures approved by the IACUC at Stanford University. Experiments were not randomized, the investigators were not blinded, and all samples/data were included in the analysis. Group sample sizes were chosen based on (1) previous experiments, (2) performance of statistics analysis, and (3) logistical reasons with respect to full study size, to accommodate all groups. Adenoviruses (E1 and E3 deleted, replication deficient) were constructed to express scFv–DKK1c or scFv–DKK1c–RSPO2 with an N-terminal signal peptide and C-terminal 6×His-tag (Ad-scFv–DKK1c or Ad-scFv–DKK1c–RSPO2), respectively. Adenoviruses expressing mouse IgG2α Fc (Ad-Fc), human RSPO2–Fc fusion protein (Ad-RSPO2–Fc) and mouse WNT3A (Ad-Wnt3a) were constructed and described in the companion paper by Yan *et al.*[26] The adenoviruses were cloned, purified by CsCl gradient, and titred as previously described[69]. Adult C57Bl/6J mice were purchased from Taconic Biosciences. Adult C57Bl/6J mice between 8–10 weeks old were injected intravenously with a single dose of adenovirus at between 1.2×10^7 p.f.u. to 6×10^8 p.f.u. per mouse in 0.1 ml PBS. Serum expression of Ad-scFv–DKK1c or Ad-scFv–DKK1c–RSPO2 were confirmed by immunoblotting using mouse anti-6×His (Abcam ab18184, 1:2,000) or rabbit anti-6×His (Abcam ab9108, 1:1,000), respectively. All experiments used $n = 4$ mice per group and repeated at least twice.

qRT–PCR on liver samples were performed as following. Total cDNA was prepared from each liver sample using Direct-Zol RNA miniprep kit (Zymo Research) and iScript Reverse Transcription Supermix for RT-qPCR (BIO-RAD). Gene expression was analysed by -$\Delta\Delta C_t$ or fold change ($2^{-\Delta\Delta C_t}$). Unpaired Student's *t*-test (two tailed) was used to analyse statistical significance. Primers for mouse *Axin2* and *Cyp2f2* were previously published[70]. Additional primers used were listed as below:

scFv-DKK1c junction F: 5′-TCAAGTACGTGTTCGCCAA-3′; R: TCAGAGGACCTCAGGCACA; scFv–DKK1c–RSPO2 junction F: 5′-ATCATCAGGCCTCCAACT-3′, R: CAACCCTTGCAAATGGGA; RSPO2–Fc F: 5′-TTGCATAGAGGCCGTTGCT-3′, R: 5′-CCATTCGCTCCAATGACCAA-3′; mouse *Glul* F: 5′-ATGCAGATAGGGTGACCACT-3′, R: 5′-GTCCATTTGCAGGAAATGGC-3′; mouse *Wnt3a* F: 5′-TACCTCTTAGTGCTCTGCAG-3′, R: 5′-CTGAGTGCTCAGAGAGGAGT-3′; mouse *Axin2*: F: 5′-GCAGGAGCCTCACCCTTC-3′, R: 5′-TGCCAGTTTCTTTGGCTCTT-3′; mouse *Cyp2f2* F: 5′-CCGGAACTTTGGAGGCATGAA-3′, R: 5′-GGTCATCAGCAGGGTATCCAT-3′.

For the parabiosis experiment, age- and gender-matched C57Bl/6J mice were housed together for at least 2 weeks before surgery. At 2 days before surgery, the 'donor' mice were injected intravenously with a single dose of adenovirus at between 1.2×10^7 pfu to 6×10^8 pfu per mouse in 0.1 ml PBS and were separated from the 'recipient' mice until surgery. The parabiosis surgery was performed as described previously[71]. The establishment of shared circulation was confirmed at day 5 after surgery by presence of adenovirus-expressed proteins in the serum of both donors and recipients.

Histological analysis and immunofluorescence. Mouse livers were collected and fixed in 4% paraformaldehyde. 5 μm paraffin-embedded sections were stained with the following antibodies after citrate antigen retrieval and blocking with 10% normal goat serum: mouse anti-glutamine synthetase antibody (Millipore MAB302, 1:200), mouse anti-PCNA (BioLegend 307902, 1:200), and rabbit anti-HNF4α (Cell Signaling 3113S, 1:500). The immunostained tissue sections were analysed and images were captured on a Zeiss Axio-Imager Z1 with ApoTome attachment.

Data availability. Atomic structure factors and coordinates have been deposited to the Protein Data Bank (PDB) under accession numbers 5UN5 and 5UN6. All other data are available from the corresponding author upon reasonable request.

32. Veeman, M. T., Slusarski, D. C., Kaykas, A., Louie, S. H. & Moon, R. T. Zebrafish prickle, a modulator of noncanonical Wnt/Fz signaling, regulates gastrulation movements. *Curr. Biol.* **13,** 680–685 (2003).
33. Biechele, T. L. & Moon, R. T. Assaying β-catenin/TCF transcription with β-catenin/TCF transcription-based reporter constructs. *Methods Mol. Biol.* **468,** 99–110 (2008).
34. Cooper, S. *et al.* Predicting protein structures with a multiplayer online game. *Nature* **466,** 756–760 (2010).
35. Azoitei, M. L. *et al.* Computation-guided backbone grafting of a discontinuous motif onto a protein scaffold. *Science* **334,** 373–376 (2011).
36. Fleishman, S. J. *et al.* RosettaScripts: a scripting language interface to the Rosetta macromolecular modeling suite. *PLoS One* **6,** e20161 (2011).
37. Whitehead, T. A. *et al.* Optimization of affinity, specificity and function of designed influenza inhibitors using deep sequencing. *Nat. Biotechnol.* **30,** 543–548 (2012).
38. Kunkel, T. A. Rapid and efficient site-specific mutagenesis without phenotypic selection. *Proc. Natl Acad. Sci. USA* **82,** 488–492 (1985).
39. Chao, G., Cochran, J. R. & Wittrup, K. D. Fine epitope mapping of anti-epidermal growth factor receptor antibodies through random mutagenesis and yeast surface display. *J. Mol. Biol.* **342,** 539–550 (2004).
40. Kabsch, W. Xds. *Acta Crystallogr. D* **66,** 125–132 (2010).
41. McCoy, A. J. *et al.* Phaser crystallographic software. *J. Appl. Crystallogr.* **40,** 658–674 (2007).
42. Emsley, P. & Cowtan, K. Coot: model-building tools for molecular graphics. *Acta Crystallogr. D* **60,** 2126–2132 (2004).
43. Adams, P. D. *et al.* PHENIX: a comprehensive Python-based system for macromolecular structure solution. *Acta Crystallogr. D* **66,** 213–221 (2010).
44. Chen, V. B. *et al.* MolProbity: all-atom structure validation for macromolecular crystallography. *Acta Crystallogr. D* **66,** 12–21 (2010).
45. Chao, G. *et al.* Isolating and engineering human antibodies using yeast surface display. *Nat. Protocols* **1,** 755–768 (2006).
46. Boder, E. T. & Wittrup, K. D. Yeast surface display for directed evolution of protein expression, affinity, and stability. *Methods Enzymol.* **328,** 430–444 (2000).
47. Los, G. V. *et al.* HaloTag: a novel protein labeling technology for cell imaging and protein analysis. *ACS Chem. Biol.* **3,** 373–382 (2008).
48. Gautier, A. *et al.* An engineered protein tag for multiprotein labeling in living cells. *Chem. Biol.* **15,** 128–136 (2008).
49. Muster, B. *et al.* Respiratory chain complexes in dynamic mitochondria display a patchy distribution in life cells. *PLoS One* **5,** e11910 (2010).
50. Löchte, S., Waichman, S., Beutel, O., You, C. & Piehler, J. Live cell micropatterning reveals the dynamics of signaling complexes at the plasma membrane. *J. Cell Biol.* **207,** 407–418 (2014)
51. Chen, B. *et al.* Small molecule-mediated disruption of Wnt-dependent signaling in tissue regeneration and cancer. *Nat. Chem. Biol.* **5,** 100–107 (2009).
52. VandeVondele, S., Vörös, J. & Hubbell, J. A. RGD-grafted poly-l-lysine-graft-(polyethylene glycol) copolymers block non-specific protein adsorption while promoting cell adhesion. *Biotechnol. Bioeng.* **82,** 784–790 (2003).
53. Vogelsang, J. *et al.* A reducing and oxidizing system minimizes photobleaching and blinking of fluorescent dyes. *Angew. Chem. Int. Ed. Engl.* **47,** 5465–5469 (2008).
54. Thompson, R. E., Larson, D. R. & Webb, W. W. Precise nanometer localization analysis for individual fluorescent probes. *Biophys. J.* **82,** 2775–2783 (2002).
55. Gould, T. J., Verkhusha, V. V. & Hess, S. T. Imaging biological structures with fluorescence photoactivation localization microscopy. *Nat. Protocols* **4,** 291–308 (2009).
56. Sergé, A., Bertaux, N., Rigneault, H. & Marguet, D. Dynamic multiple-target tracing to probe spatiotemporal cartography of cell membranes. *Nat. Methods* **5,** 687–694 (2008).
57. Schütz, G. J., Schindler, H. & Schmidt, T. Single-molecule microscopy on model membranes reveals anomalous diffusion. *Biophys. J.* **73,** 1073–1080 (1997).
58. You, C. *et al.* Electrostatically controlled quantum dot monofunctionalization for interrogating the dynamics of protein complexes in living cells. *ACS Chem. Biol.* **8,** 320–326 (2013).
59. Wedeking, T. *et al.* Single cell GFP-trap reveals stoichiometry and dynamics of cytosolic protein complexes. *Nano Lett.* **15,** 3610–3615 (2015).
60. Shah, S. M., Kang, Y. J., Christensen, B. L., Feng, A. S. & Kollmar, R. Expression of Wnt receptors in adult spiral ganglion neurons: frizzled 9 localization at growth cones of regenerating neurites. *Neuroscience* **164,** 478–487 (2009).
61. Zhong, Z. A., Ethen, N. J. & Williams, B. O. Use of primary calvarial osteoblasts to evaluate the function of Wnt signaling in osteogenesis. *Methods Mol. Biol.* **1481,** 119–125 (2016).
62. van de Wetering, M. *et al.* Prospective derivation of a living organoid biobank of colorectal cancer patients. *Cell* **161,** 933–945 (2015).
63. Sato, T. *et al.* Long-term expansion of epithelial organoids from human colon, adenoma, adenocarcinoma, and Barrett's epithelium. *Gastroenterology* **141,** 1762–1772 (2011).
64. Bartfeld, S. *et al. In vitro* expansion of human gastric epithelial stem cells and their responses to bacterial infection. *Gastroenterology* **148,** 126–136 (2015).
65. Stange, D. E. *et al.* Differentiated Troy$^+$ chief cells act as reserve stem cells to generate all lineages of the stomach epithelium. *Cell* **155,** 357–368 (2013).
66. Boj, S. F. *et al.* Organoid models of human and mouse ductal pancreatic cancer. *Cell* **160,** 324–338 (2015).
67. Huch, M. *et al.* Unlimited in vitro expansion of adult bi-potent pancreas progenitors through the Lgr5/R-spondin axis. *EMBO J.* **32,** 2708–2721 (2013).
68. Huch, M. *et al.* Long-term culture of genome-stable bipotent stem cells from adult human liver. *Cell* **160,** 299–312 (2015).
69. Wei, K. *et al.* A liver Hif-2α–Irs2 pathway sensitizes hepatic insulin signaling and is modulated by Vegf inhibition. *Nat. Med.* **19,** 1331–1337 (2013).
70. Rocha, A. S. *et al.* The angiocrine factor Rspondin3 is a key determinant of liver zonation. *Cell Reports* **13,** 1757–1764 (2015).
71. Wagers, A. J., Sherwood, R. I., Christensen, J. L. & Weissman, I. L. Little evidence for developmental plasticity of adult hematopoietic stem cells. *Science* **297,** 2256–2259 (2002).

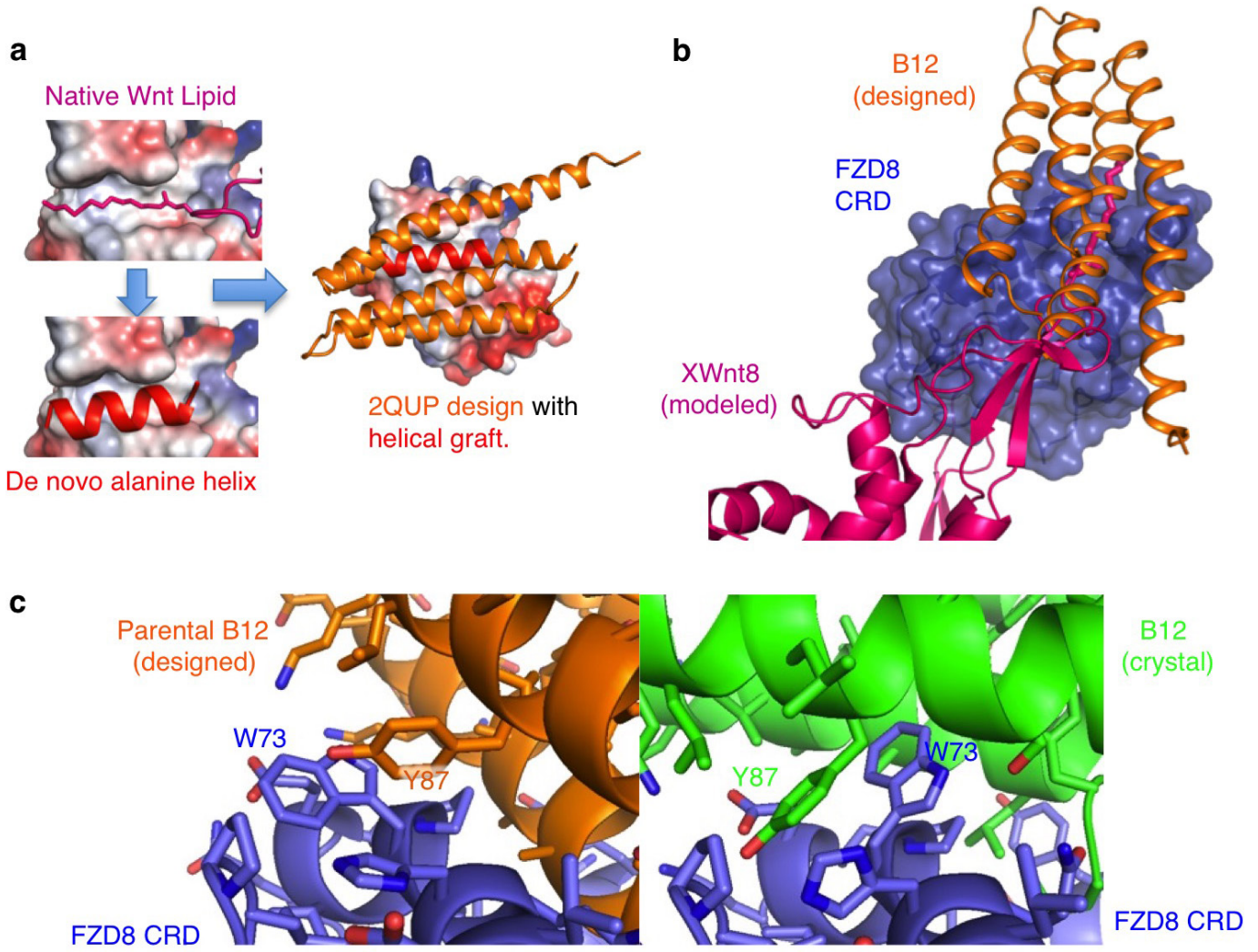

d

Position	26	48	53	56	57	63	88	117	120	121	122
Parental B12 AA	K	A	A	A	A	K	K	L	R	I	Y
Enriched AA	I	V	L/T	L	Q	P	L	T/I	S	G/V	P
Selected AA	**I**	**V**	**T**	**L**	**Q**	**P**	**L**	**T**	R	**V**	Y

Extended Data Figure 1 | *De novo* design and engineering of B12. **a**, Design strategy of a FZD8 CRD-specific binding domain. **b**, Designed binding of B12 (orange) to the FZD8 CRD (blue), with XWnt8 and Wnt lipid (purple) modelled onto the structure to highlight competitive binding modes. Residues outside of the 'lipid groove helix' were designed to make FZD8-specific contacts to promote specificity. **c**, Comparison between the designed (left) and observed (right) conformation. **d**, Affinity maturation of parental B12 by yeast cell surface display identified enriched point mutations that were assembled in a degenerate library and selected to yield the final, optimized B12.

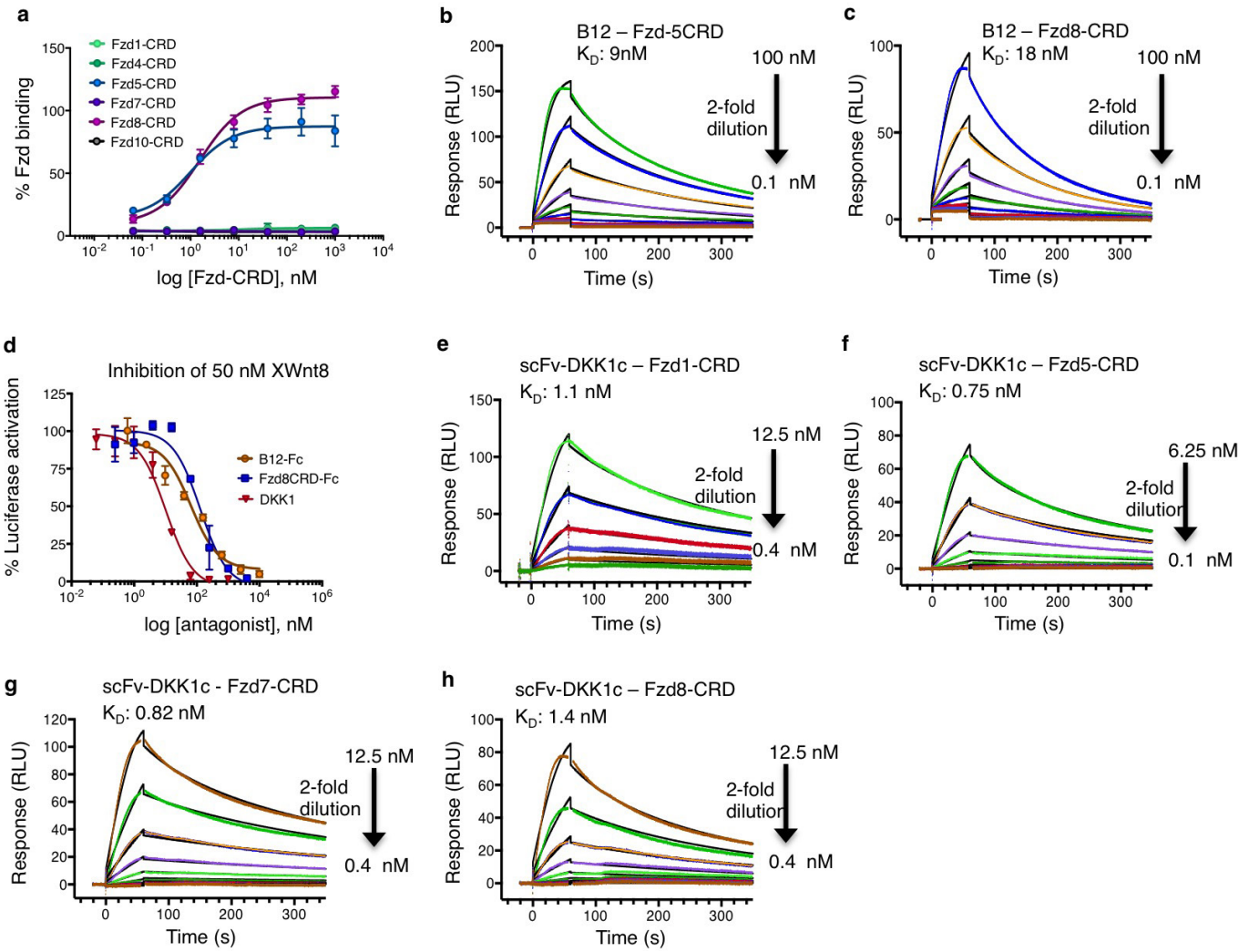

Extended Data Figure 2 | FZD CRD binding characterization of B12 and scFv. a, Binding specificity of the B12 and FZD CRD interaction, as determined by yeast cell surface titration. B12 was displayed on yeast and binding of monomeric FZD CRDs fluorescently labelled with streptavidin-Alexa647 was detected by flow cytometry. Error bars represent s.d. of $n = 3$ technical replicates from 1 of 2 representative experiments. **b**, **c**, Binding affinity of the B12–FZD5 CRD (**b**) and B12–FZD8 CRD (**c**) interaction, as determined by surface plasmon resonance. FZD5 and FZD8 CRDs were immobilized on a streptavidin chip, and B12 was flown through as analyte. **d**, Inhibition of XWnt8 induced signalling in A549 cells, as measured by BAR luciferase reporter assay. Error bars represent s.d. of $n = 3$ technical replicates from 1 of 2 representative experiments. **e**–**h**, Binding affinity of the scFv–DKK1c–FZD1 CRD (**e**). scFv–DKK1c–FZD5 CRD (**f**), scFv–DKK1c–FZD7 CRD (**g**) and scFv–DKK1c–FZD8 CRD (**h**) interaction, as determined by surface plasmon resonance. FZD CRDs were immobilized on a streptavidin chip, and scFv–DKK1c was flown through as analyte.

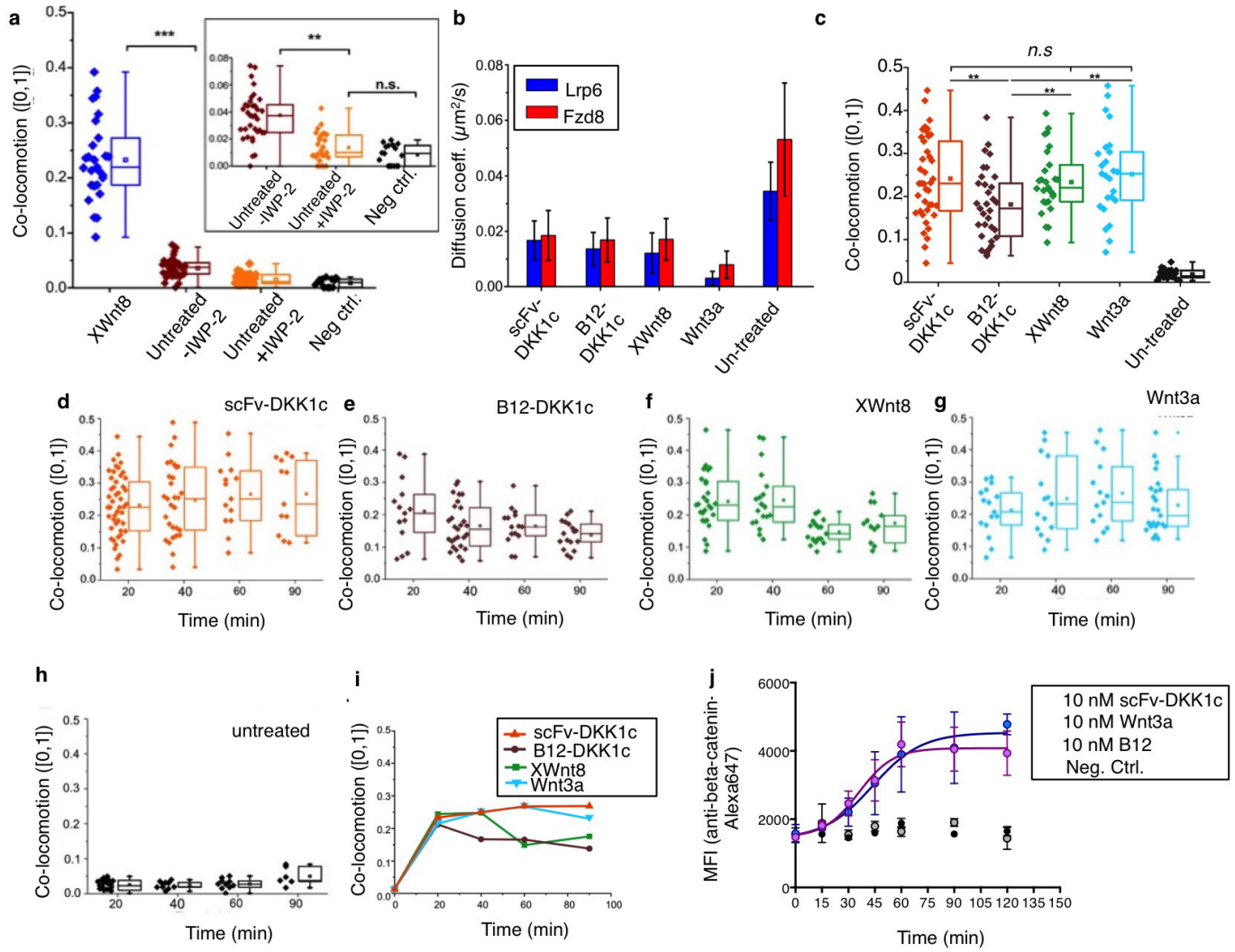

Extended Data Figure 3 | Co-locomotion analysis of LRP6 and FZD8 induced by Wnt protein and surrogate. a, Dimer/oligo-merization of LRP6 and FZD8 quantified by co-locomotion of both receptors under different conditions. The negative control (black) is the dimerization of DY649-labelled FZD8 and a TMR-labelled model transmembrane protein, HaloTag with maltose-binding protein linked to an artificial transmembrane domain, co-expressed in HeLa cells. The addition of 2 μM IWP-2 for 20 h reduced the receptor dimerization to the background level of the negative control (inset). Receptor dimerization induced by XWnt8 was used as a positive control (blue). Box plot represents measurements of more than 18 individual cells for each condition. $^{**}P < 0.01$, $^{***}P < 0.001$, *t*-test. **b**, Diffusion coefficients of LRP6 and FZD8 in the absence or presence of 100 nM Wnt surrogates and control Wnt proteins. Error bars represent s.d. from more than 25 individual cells. **c**, Co-locomoting LRP6 and FZD8 measured within 30 min of the addition of 100 nM scFv–DKK1c, B12–DKK1c, XWnt8 and WNT3A, or without treatment. Box plot represents measurements of individual cells for each condition ($^{**}P < 0.01$, *t*-test). scFv–DKK1c ($n = 40$), B12–DKK1c ($n = 32$), XWnt8 ($n = 27$), WNT3A ($n = 25$), and untreated ($n = 28$). **d**–**i**, Dimer/oligo-merization of LRP6 and FZD8 as a function of time after the addition of 100 nM scFv–DKK1c (**d**), B12–DKK1c (**e**), XWnt8 (**f**) and WNT3A (**g**). More than 12 individual cells were evaluated for each condition. **h**, Time course control of untreated cell. **i**, Summarized representation of time course of LRP6–FZD8 complex formation. **j**, Kinetics of β-catenin accumulation in K562 cells after stimulation with 10 nM scFv–DKK1c, recombinant WNT3A, B12, or basal conditions only (complete growth medium). Error bars represent s.d. of $n = 3$ technical replicates from 1 of 2 representative experiments.

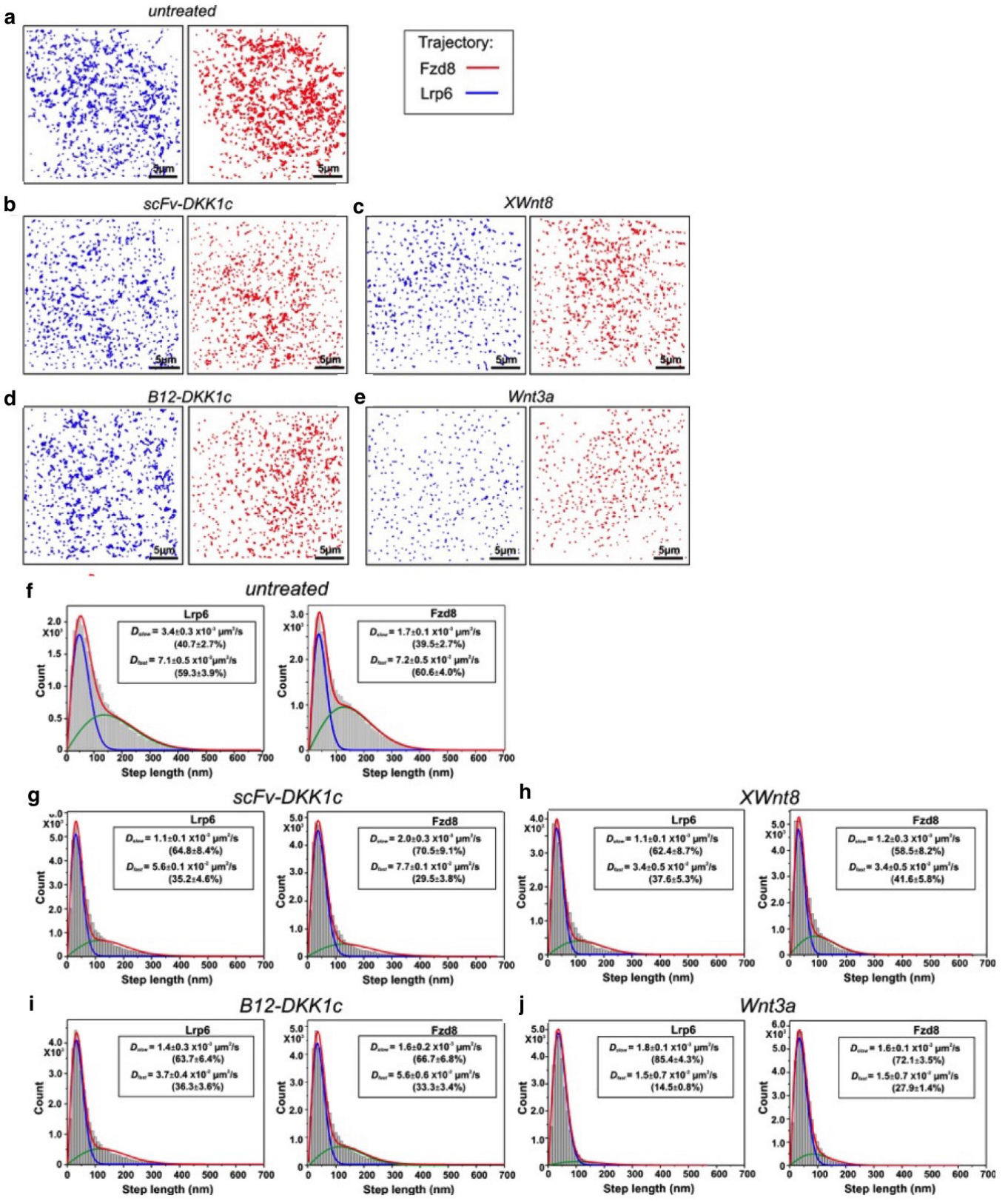

Extended Data Figure 4 | Single-molecule trajectories and step length analysis of LRP6 and FZD8 under different conditions. **a**–**e**, Single-molecule trajectories obtained for LRP6 and FZD8 in the plasma membrane of representative HeLa cells under different conditions. Trajectories were obtained by single-molecule tracking of the dye-labelled LRP6 (blue) and FZD8 (red) in the dual-colour time-lapse single-molecule images within 150 frames. Fast diffusion results into spread-out trajectories (prominent in **a**), while slow diffusion leads to dot-like trajectories (prominent in **e**). **f**–**j**, Step-length histogram analyses for determining diffusion coefficients of LRP6 and FZD8, shown for representative individual cells under different conditions. Step lengths for a time lapse of three frames (96 ms) were calculated from trajectories shown in **a**–**e**. According to equation (1), a two-component model comprising a slow (blue) and a fast (green) fraction was used for fitting the histograms. Inset: diffusion coefficient and the corresponding fraction in percentage (in brackets).

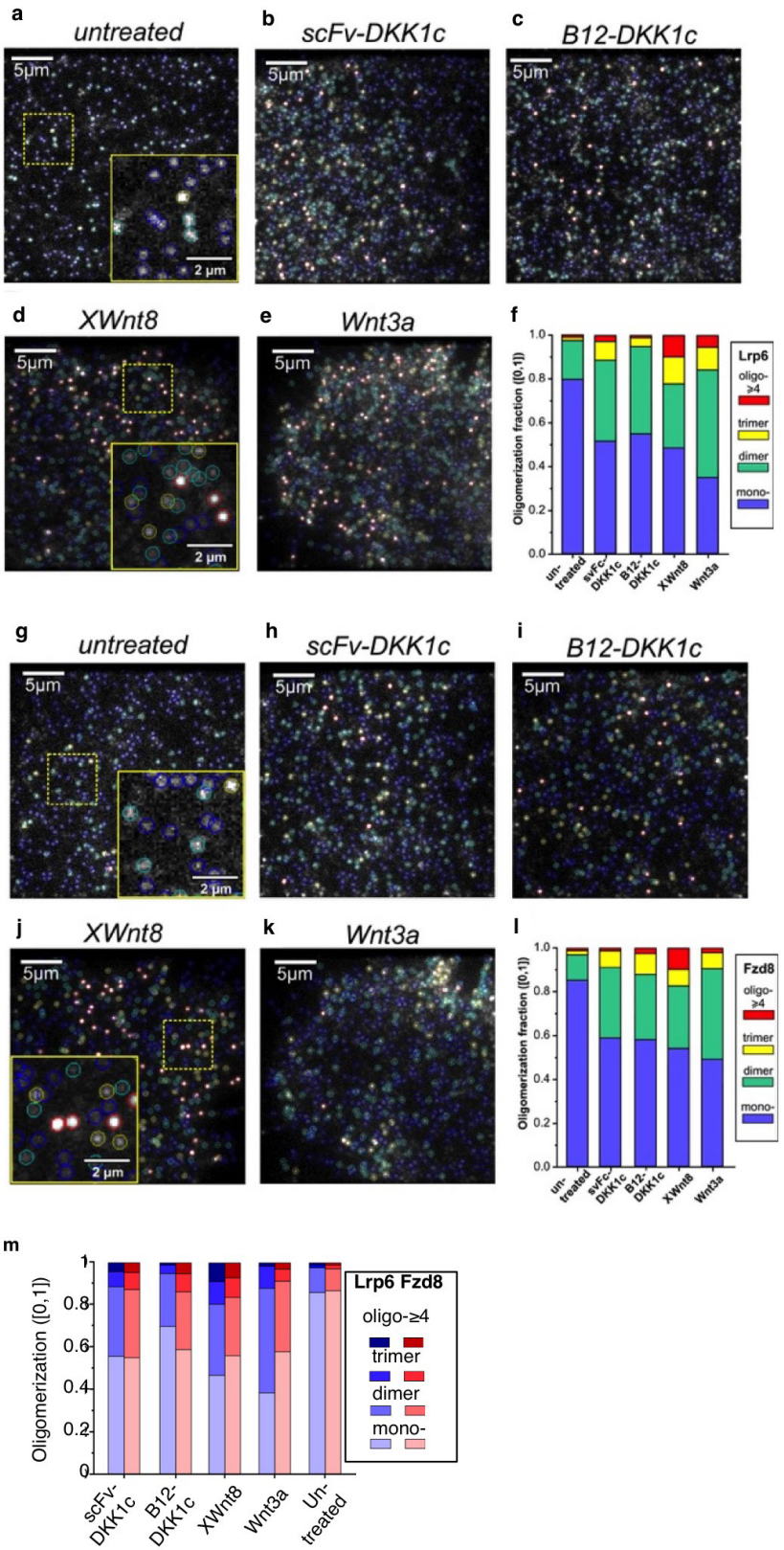

Extended Data Figure 5 | Single-molecule intensity analysis of LRP6 and FZD8 under different conditions. Single-molecule intensity analysis for quantifying LRP6 (**a**–**f**) and FZD8 (**g**–**l**) oligomerization in representative cells under different conditions. Raw images after treatment with scFv–DKK1c (**b**, **h**), B12–DKK1c (**c**, **i**), XWnt8 (**d**, **j**), WNT3A (**e**, **k**) and without treatment (**a**, **g**). On the basis of their intensities, individual diffraction-limited spots in the raw images were classified as monomers (blue circle), dimers (green circle), trimers (yellow circle) and higher oligomers (red circle), respectively. **f**, **l**, **m**, Different oligomer fractions summarized as the ratio of the classified species number to the total number of detected diffraction-limited spots. More than 7,200 single complex intensities were examined for each condition.

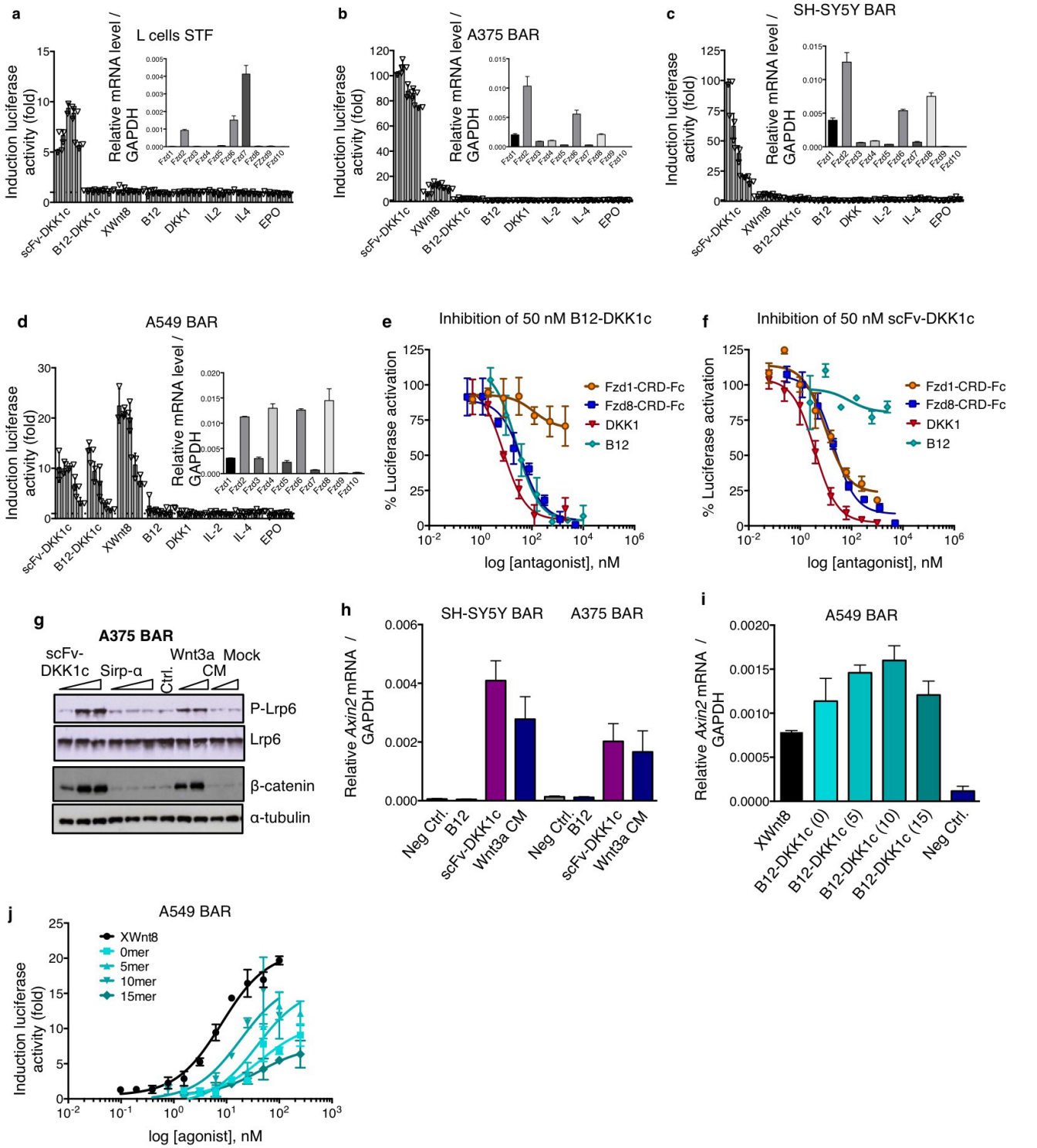

Extended Data Figure 6 | FZD-specific activation of canonical Wnt signalling by Wnt surrogates. a–d, Activation of Wnt pathway by decreasing concentration of scFv–DKK1c, B12–DKK1c, XWnt8 or negative control proteins B12, DKK1, IL-2, IL-4 and EPO, as assayed by the BAR and STF reporters in L cells (50–3 nM) (**a**), A375 cells (250–15 nM) (**b**), SH-SY5Y cells (250–15 nM) (**c**) and A549 cells (100–1 nM) (**d**). Error bars represent s.d. of $n = 3$ technical replicates from 1 of 2 representative experiments. The relative quantities of human *FZD* mRNA in the relative cell lines determined by qRT–PCR are shown as insets, error bars represent s.d. of $n = 3$ technical replicates. **e**, **f**, Selective inhibition of B12–DKK1c and scFv–DKK1c activity in A549 cells by B12, DKK1, FZD1 CRD–Fc and FZD8 CRD–Fc, as assayed by the BAR reporter, correlates with binding specificity. Error bars represent s.d. of $n = 3$ technical replicates. **g**, Immunoblot analysis of LRP6 phosphorylation and β-catenin accumulation in A375 BAR cells treated with scFv–DKK1c and human SIRPα (0.1, 10, 50 nM), WNT3A conditioned media and mock conditioned media (30% and 50%). Data shown from 1 of 2 representative experiments. **h**, *AXIN2* transcription relative to *GAPDH* in SH-SY5Y BAR and A375 BAR cells treated with 50 nM scFv–DKK1c, B12 (negative control), and 30% WNT3A conditioned media, as analysed by qRT–PCR. Error bars represent the s.d. of biological triplicates performed in technical triplicates ($n = 9$). **i**, *AXIN2* transcription relative to *GAPDH* in A549 BAR cells treated with 50 nM B12–DKK1c variants and XWnt8, as analysed by qRT–PCR. Error bars represent s.d. of biological triplicates performed in technical triplicates ($n = 9$). **j**, Activation of Wnt signalling with distinct amplitudes by XWnt8 and B12–DKK1c variants, as assayed by the BAR reporter in A549 cells. Error bars represent s.d. of $n = 3$ technical replicates from 1 of 3 representative experiments.

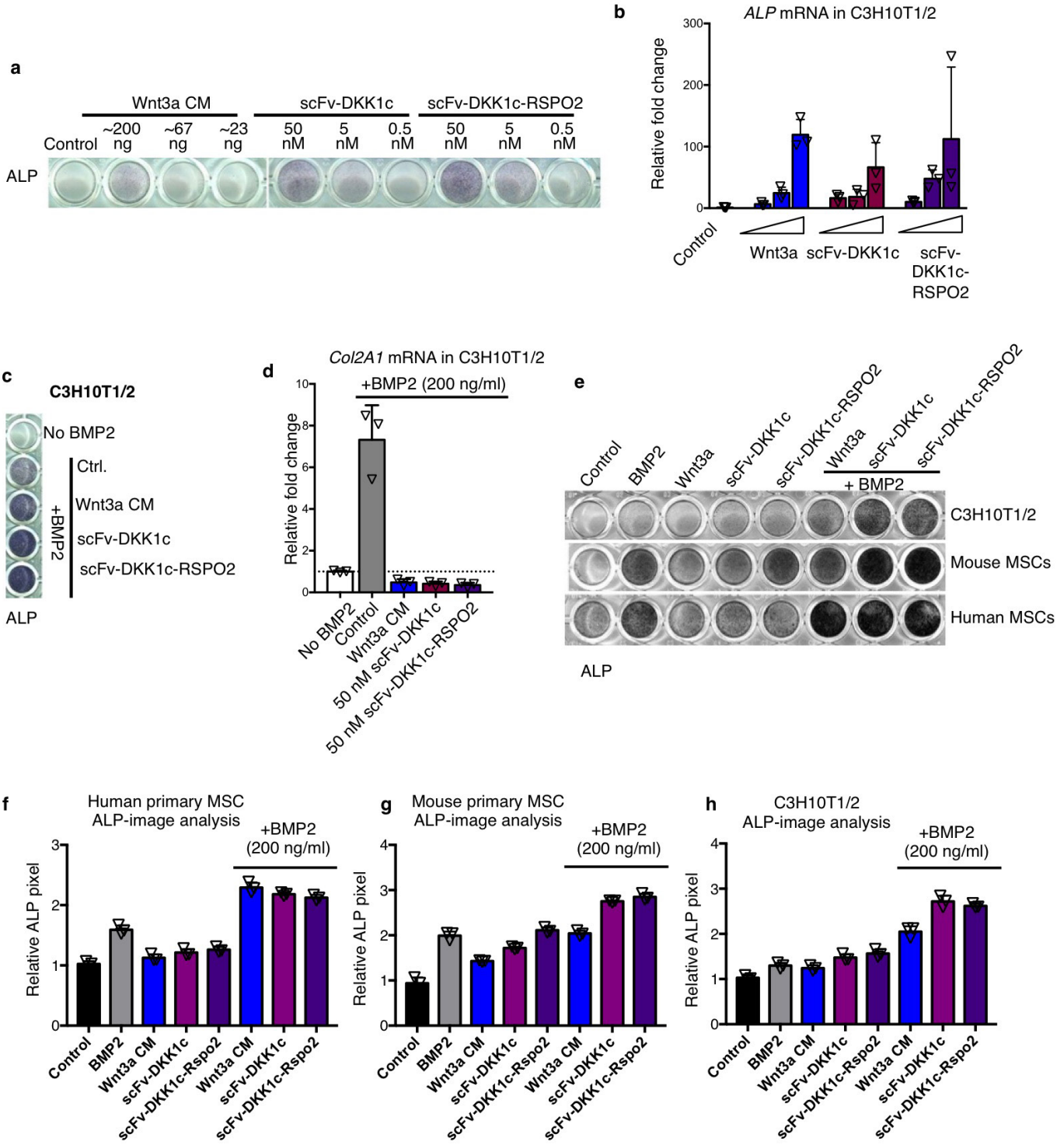

Extended Data Figure 7 | Wnt surrogates enhance upregulation of alkaline phosphatase in MSCs. Upregulation of alkaline phosphatase (ALP) assessed by the cell surface enzymatic activity with the ALP substrate NBT/BCIP (**a**), and qRT–PCR of mRNA levels (**b**) in C3H10T1/2 cells treated for 4 days with increasing concentration of WNT3A conditioned media, scFv–DKK1c (0.5, 5, 50 nM) and scFv–DKK1c–RSPO2 (0.5, 5, 50 nM) in osteogenic media. **c**, Induction of ALP in C3H10T1/2 cells treated with WNT3A conditioned media, 50 nM scFv–DKK1c and 50 nM scFv–DKK1c–RSPO2 in the presence of 200 ng ml^{-1} BMP2 in osteogenic media for 4 days, assayed by cell-surface ALP enzymatic activity with the ALP substrate NBT/BCIP. **d**, Relative changes of *Col2a1* mRNA levels, an early marker of chondrogenesis, in C3H10T1/2 cells treated with WNT3A conditioned media, scFv–DKK1c and scFv–DKK1c–RSPO2 in the presence of BMP2 in osteogenic media for 4 days. **e**, Upregulation of ALP cell surface enzymatic activity assessed with the ALP substrate NBT/BCIP in C3H10T1/2, mouse primary MSCs, and human primary MSCs treated for 3 days with WNT3A conditioned media, 50 nM scFv–DKK1c, and 50 nM scFv–DKK1c–RSPO2 in osteogenic media in the presence and absence of 200 ng ml^{-1} BMP2. **f**–**h**, Pixel quantification of images in **e** using ImageJ. Error bars represent s.d. of $n = 3$ technical replicates from 1 of 3 (C3H10T1/2 and human MSCs) and 1 (mouse MSCs) representative experiments.

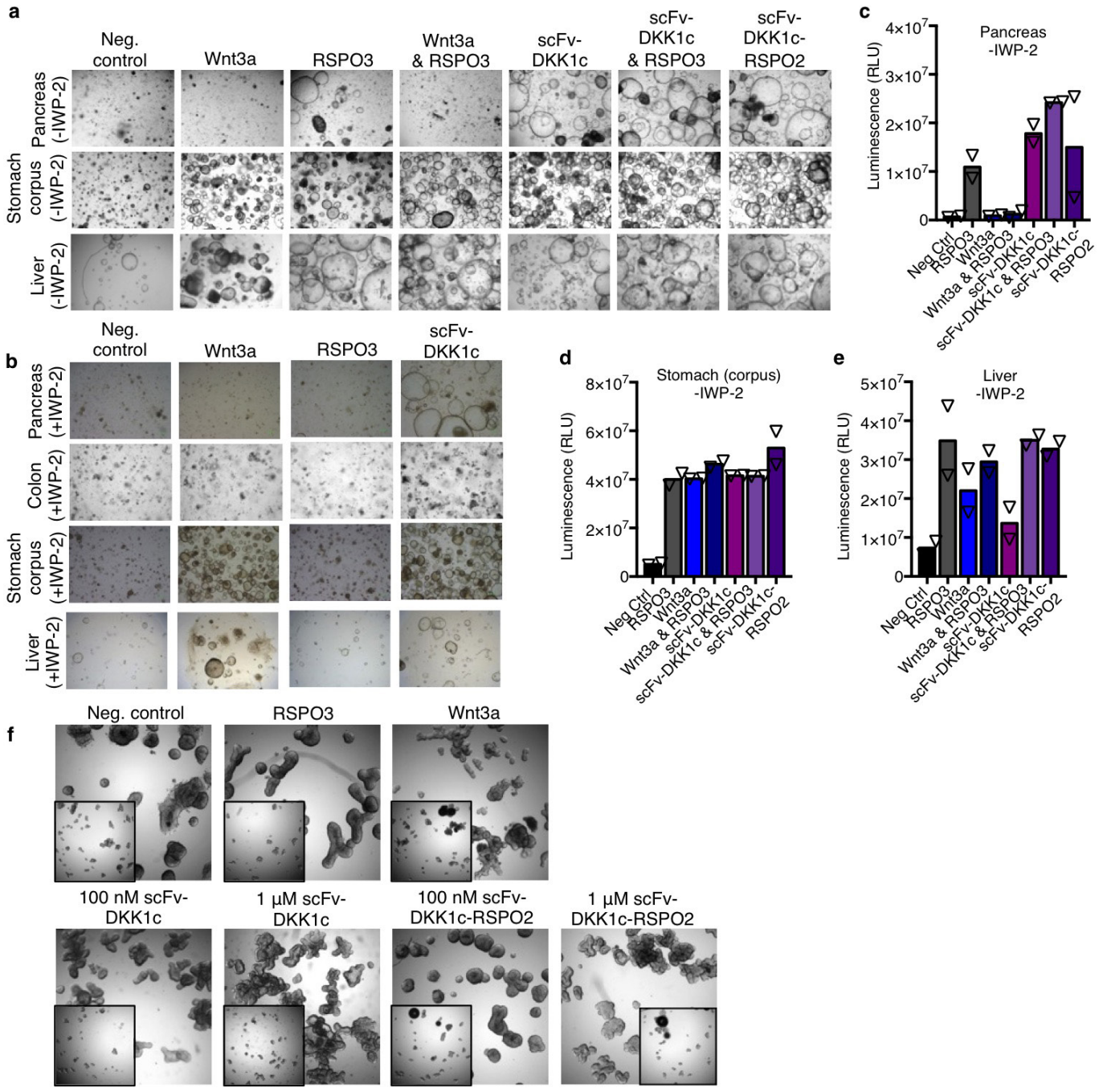

Extended Data Figure 8 | Activity of Wnt surrogates on human organoid cultures *in vitro*. **a**, **b**, Representative bright-field images of organoids of human pancreas, stomach (corpus), and liver expanded for 12 days in the absence (**a**) or presence (**b**) of 3 µM IWP-2 in basal media (as detailed in Supplementary Table 2), supplemented with 50% WNT3A conditioned media, 2% RSPO3 conditioned media, 200 nM scFv–DKK1c and 200 nM scFv–DKK1c–RSPO2, or combinations thereof as indicated. **c**–**e**, Quantification of cell proliferation by luminescence. Bars represent mean of $n = 2$ technical replicates from 1 of 3 (colon), 2 (liver and pancreas) and 1 (stomach) representative experiments. **f**, Representative bright-field images of colon organoids from a patient with cystic fibrosis with characteristic budded morphology owing to mutations in the ion channel CFTR, grown in expansion media with 50% WNT3A conditioned media, 2% RSPO3 conditioned media, 100 and 1,000 nM scFv–DKK1c and 100 and 1,000 nM scFv–DKK1c–RSPO2, or combinations thereof as indicated.

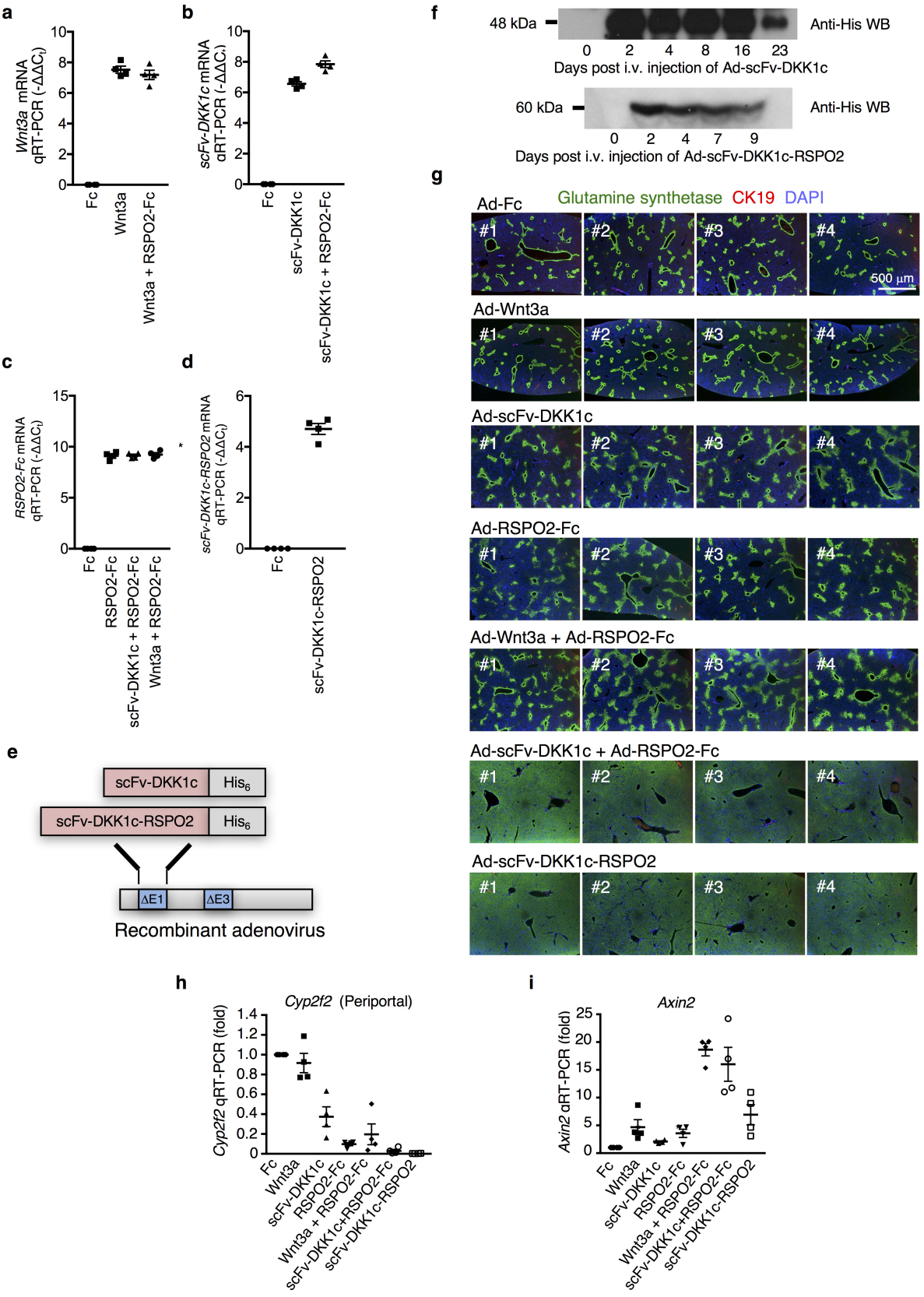

Extended Data Figure 9 | See next page for caption.

Extended Data Figure 9 | Wnt surrogate activate Wnt signalling *in vivo* and alter Wnt-driven hepatic zonation. a–d, qRT–PCR validation of adenoviral transgene expression in mouse livers 7 days after intravenous injection with Ad-Wnt3a, Ad-scFv–DKK1c, Ad-RSPO2–Fc or Ad-scFv–DKK1c–RSPO2 from the same experiment as in **g**. $n = 4$ mice per condition. **e**, Schematic representation of Ad-scFv–DKK1c and Ad-scFv-DKK1c-RSPO2 constructs for adenoviral transgene expression. **f**, Detection of scFv–DKK1c and scFv–DKK1c–RSPO2 in mice sera by western blot at the indicated days after adenovirus injection. **g**, Images from biological replicate mice depicting effects of adenoviral expression of various Wnt agonists on liver zonation from Fig. 4a, b. Mice ($n = 4$ per condition) received single intravenous injection of adenovirus expressing Fc (2.5×10^8 p.f.u.), scFv–DKK1c (1.2×10^7 p.f.u.), WNT3A (1.2×10^7 p.f.u.), RSPO2–Fc (2.5×10^8 p.f.u.), scFv–DKK1c–RSPO2 (1.2×10^7 p.f.u.), or combinations as indicated. In all cases, the total virus dose was increased to 2.5×10^8 p.f.u. by Ad-Fc as filler. After 7 days, liver was analysed for glutamine synthetase expression by immunofluorescence. Anti-CK19 immunofluorescence was performed to mark portal areas. Each panel is a representative image from a different mouse. **h**, **i**, qRT–PCR analysis of periportal marker *Cyp2f2* (**h**) and Wnt target gene *Axin2* (**i**) in livers from mice that received adenoviruses expressing the mouse IgG2α Fc fragment, mouse WNT3A, scFv–DKK1c, human RSPO2–Fc, WNT3A plus RSPO2–Fc, scFv–DKK1c plus RSPO2–Fc or scFv–DKK1c–RSPO2, 7 days after adenovirus injection ($n = 4$ mice per group). Error bars indicate s.e.m. of biological replicates.

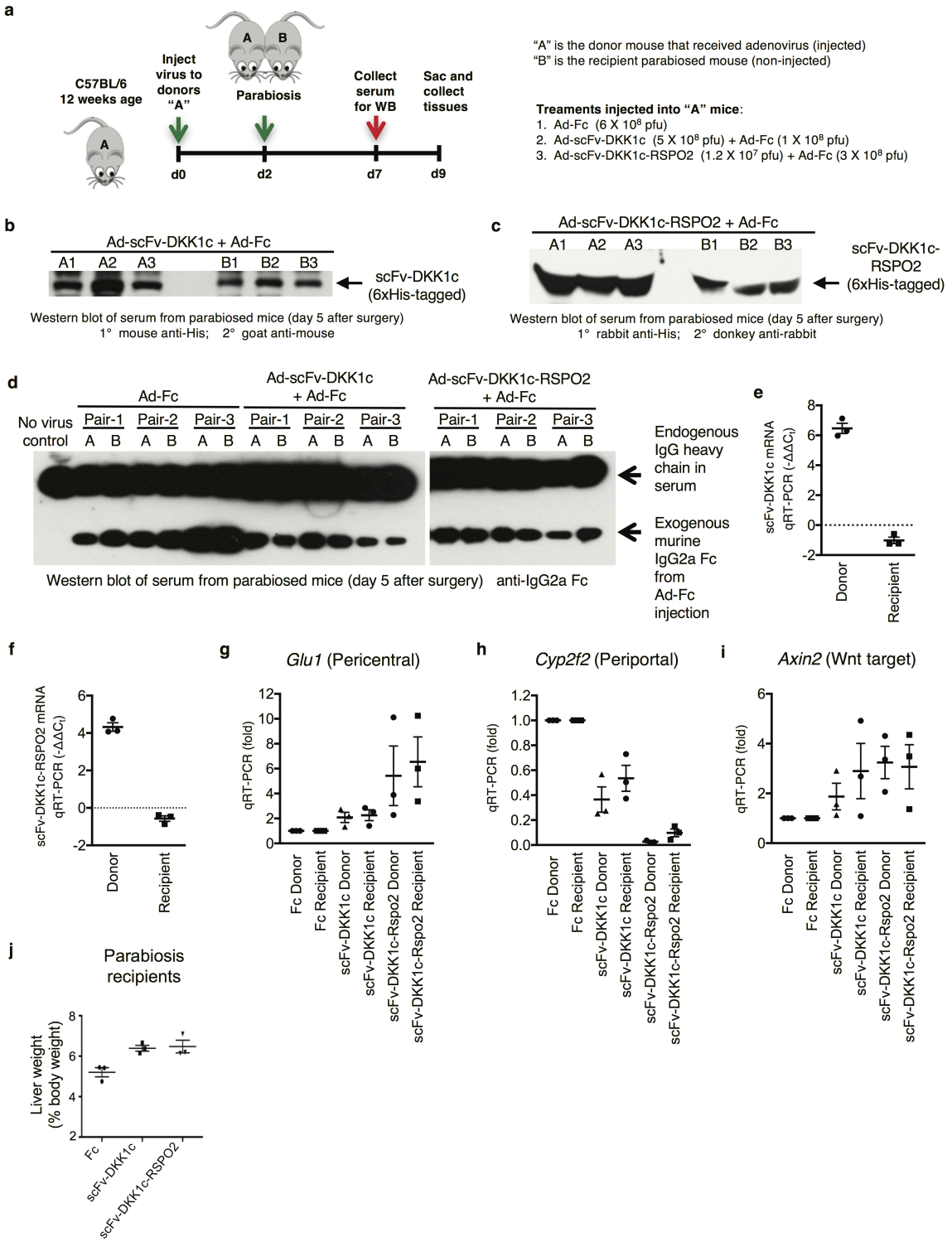

Extended Data Figure 10 | Wnt surrogate enhance hepatocyte proliferation. a, Scheme depicting parabiosis experiment design. Age-matched and gender-matched mice were selected and housed together. The donors received intravenous adenovirus injection of (1) Ad-Fc, (2) Ad-scFv–DKK1c-His plus Ad-Fc or (3) Ad-scFv–DKK1c–RSPO2 plus Ad-Fc with liver infection of the donors. Two days later, parabiosis surgery was performed to surgically pair the adenovirus injected donor mice with the recipient mice that did not receive adenovirus injection. Ad-Fc was deliberately added to all treatment groups as a tracer to monitor the successful establishment of cross-circulation (see **b**). **b**–**d**, Detection of scFv–DKK1c (**b**), scFv–DKK1c–RSPO2 (**c**) or the tracer Fc (**d**) in the serum of recipients and donor mice 5 days after parabiosis by western blotting. **e**, **f**, Liver qRT–PCR validation of adenoviral transgene expression from donor and recipient mice at 7 days after surgery (9 days after adenoviral injection) for scFv–DKK1c or scFv–DKK1c–RSPO2. Note the absence of transgene expression in the recipient livers. **g**–**i**, Analysis of livers by qRT–PCR for *Glul*, *Cyp2f2* and *Axin2* mRNA with induction of *Glul* and *Axin2* and repression of *Cyp2f2* in both donors and recipients. **j**, Liver weight of recipients 7 days after parabiosis surgery. $n = 3$ mice per condition. Error bars indicate s.e.m. of biological replicates.